Biophysical Chemistry 5 (1976) 107–135

SIMULATION OF GRADIENT AND BAND PROPAGATION IN THE CENTRIFUGE

W.K. SARTORY, H.B. HALSALL* and J.P. BREILLATT
Molecular Anatomy (MAN) Program‡, and Reactor Division, Oak Ridge National Laboratory‡, Oak Ridge, Tennessee 37830, USA

A technique is developed for simulating the behavior of both the gradient-forming solute and macromolecular bands in a centrifuge.

The change with time of the density gradient due to diffusion and sedimentation of the gradient-forming solute is calculated by a finite difference method, making use of the results of earlier work on the theory of the equilibrium density gradient.

Using a perturbation technique, the concentration profiles of dilute bands of macromolecules are then calculated as they sediment and diffuse through the varying supporting gradient.

Results of the simulation techniques are compared with experiment.

1. Introduction

Svedberg developed his first analytical ultracentrifuge 50 years ago to quantitatively measure the sedimentation of particles in a centrifugal field. For decades these measurements were made almost exclusively in optical centrifuges relying on self-generated gradients of the particles themselves for stability. Zone sedimentation, however, requires a separate density gradient to support the particle zone. Since most zonal centrifugations are not carried out in optical rotors, predictive and retrospective analyses of the particle zone movement in the gradient requires detailed knowledge of the gradient parameters. For this reason methods for centrifugal separations in density gradients are usually developed empirically. Optimization of these methods involves exceptional insight, long experience, or numerous experiments to evaluate all parameters. When the K-series zonal centrifuges [1] are used for large-scale separations, such investigation of parameters is often impractical due to the expense of gradient and sample materials.

In this paper we introduce a simulation technique for use in determining the efficacy of proposed separations and to aid in optimizing the experimental parameters before the first experiment.

There are two aspects to the simulation: prediction of the behavior of the gradient-forming solute, which tends to diffuse and sediment during a run, and prediction of the behavior of the bands of macromolecules themselves. These two aspects present different problems and were approached in different ways.

Two approximations underlie both aspects. First, the bands of macromolecules are assumed to be dilute so that the concentration of macromolecules does not affect the behavior of either the gradient-forming solute or of the bands. The gradient-forming solute, however, is not considered dilute. Second, the effect of pressure on the properties has been neglected. The behavior of the gradient-forming solute will be taken up first.

Finite difference methods for the numerical calculation of sedimentation and diffusion in a centrifuge have been developed by a number of investigators [2–9]. While these authors have been primarily interested in calculating the behavior of macromolecules, their methods are applicable to solutes of arbitrary diffusivity and sedi-

* Present Address: Department of Chemistry, University of Cincinnati, Cincinnati, Ohio 45221.
‡ Supported by the National Cancer Institute, the National Institute of Allergy and Infectious Diseases, and the Energy Research and Development Administration.
‡ Operated for the Energy Research and Development Administration by Union Carbide Corporation Nuclear Division.

mentation coefficient, and can therefore also be used to study the behavior of a gradient-forming solute.

In a parallel line of investigation, the theory of the equilibrium density distribution of a gradient-forming solute has been developed [10–12]. The equilibrium distribution depends on a thermodynamic parameter, β, which can be determined from solution activity coefficients. Values of β have been tabulated as a function of concentration for a number of common gradient-forming solutes in the above papers.

In the present work we develop a finite difference method which makes use of the gradient solution diffusivity and β, to calculate the development of the density gradient with time, beginning with an arbitrary initial density distribution.

The paths followed by particles sedimenting through an arbitrary (but fixed) gradient have been calculated by numerical integration by Martin and Ames [13] and Bishop [14]. In the present work, numerical integration is used to determine the path of a particle sedimenting through a time-dependent gradient (which is itself sedimenting and diffusing). We next take up the problem of determining the concentration profile of the band of particles.

Analytic solutions to the Lamm equation describing the sedimentation and diffusion of a band of macromolecules in a centrifuge have been obtained by Gehatia and Katchalski [15], Rubin and Katchalski [16], Vinograd et al. [17], and Dishon et al. [18], by neglecting the effect of the variation in gradient properties on the propagation of the band.

Another approach to the calculation of band behavior is the method of moments [19,20]. A technique closely related to the method of moments has been used by Schumaker and Rosenbloom [21]. There is a connection between the method of moments and the eigenfunction expansion method which is developed in this work. In fact, if a complete set of moments is obtained by any technique, the eigenfunction expansion can (in principal if not in practice) be used to reconstruct the concentration profile. This method of constructing concentration profiles from moments has been applied in chromatography theory by Kucera [22].

The method of moments can be used to account for the effect of the gradient on the behavior of the band by representing the sedimentation velocity and diffusivity as a Taylor series in radius. In general, however, (if the series for sedimentation velocity is carried higher than the first power) this approach leads to recursive equations for the moments, so that each moment depends on higher moments. This recursiveness poses difficulties in solution. If the eigenfunction expansion technique of this work is interpreted as a variant of the method of moments, then we have resolved the recursiveness by a small perturbation method.

Solution of the Lamm equation by finite difference methods has also been used to calculate the behavior of a band of macromolecules [2–9]. Such methods are very general in application, and could certainly be used for the simultaneous solution of the equation governing the behavior of the desnity gradient and the bands. In the case of very narrow bands moving through a much wider gradient, difficulty would probably be encountered in choosing compatible finite-difference grids while still maintaining computational efficiency. We prefer to develop an approximate analytic solution governing the band behavior and to couple it to a finite-difference solution for the density gradient.

Sedimentation of macromolecules through an arbitrary, fixed gradient (i.e., a gradient which does not itself sediment or diffuse) has been considered by De Duve et al. [23] and Berman [24]. These authors have not considered the diffusion of the macromolecules.

An analytic solution for non-diffusive sedimentation of a band of macromolecules through a time-dependent gradient has been obtained by Dishon et al. [25]. In the same work, an analytic solution for the diffusion and sedimentation of a band through a time-dependent gradient has been obtained using the rectangular approximation. The solution technique, however, depends on the special assumed form of the time and radius dependence of the density gradient.

Weiss and Dishon [26] use a perturbation technique to calculate the diffusional spreading of a moving boundary sedimenting through an arbitrary but fixed gradient. They first obtain an exact solution in the absence of diffusion. An approximate correction for the effect of diffusion is obtained by taking the diffusivity to be a "small" parameter.

In the present work we develop a method of obtaining an approximate analytic solution for the sedimentation

and diffusion of a thin, dilute band of macromolecules through a prescribed gradient with arbitrary time and radius dependence. Both the sedimentation velocity and the diffusivity of the macromolecule are considered to be affected by the gradient. The concentration of the macromolecule is considered to be too small to have an affect on the results. A perturbation technique is used in which the band width is considered to be a "small" parameter.

2. Theory

2.1. Gradient behavior

In the present work, the diffusion and sedimentation of the gradient-forming solute and the sedimentation of the macromolecules occur simultaneously. The macromolecules, however, are assumed to be sufficiently dilute as to have no effect on the behavior of the gradient-forming solute.

The centrifuge geometry is assumed to be perfectly cylindrical or sectorial.

At equilibrium in a centrifuge, the "total potential" of the components, i.e., the sum of the chemical potential and centrifugal potential is a constant [27], so that, neglecting any axial or angular dependence:

$$\frac{\partial}{\partial r}\left(\mu_1 - \tfrac{1}{2}\omega^2 r^2\right) = 0, \tag{1}$$

where μ_1 is the chemical potential per unit mass of the gradient-forming solute, ω is the angular velocity of the rotor, and r is the radial distance from the axis of rotation (all quantities may be expressed in CGS units unless otherwise noted). If the left hand side of eq. (1) does not vanish, a flux occurs in the centrifuge.

The theory of diffusion based on irreversible thermodynamics [28] gives the radial flux in a binary solution proportional to the left-hand side of eq. (1),

$$J_1^{\mathrm{v}} = K(\omega^2 r - \partial\mu_1/\partial r), \tag{2}$$

where J_1^{v} is the mass flux of the solute relative to the volume-mean velocity of the fluid, and K is a proportionality constant.

The chemical potential depends on pressure and composition (and temperature, which we ignore by considering only an isothermal process). The composition can be specified in various ways, e.g., mass fraction, molarity, etc. It is convenient here, however, to characterize the composition of the binary gradient-forming solution by its density at atmospheric pressure, ρ^0. The difference between the density, and most of the other properties, at atmospheric pressure and at the centrifuge pressure is rather small, and we shall eventually neglect it. We retain the distinction here so that ρ^0 determines the composition independently of pressure). Eq. (2) then becomes

$$J_1^{\mathrm{v}} = K\left\{\omega^2 r - \left(\frac{\partial\mu_1}{\partial p}\right)_{\rho^0,T_{\mathrm{K}}}\frac{\partial p}{\partial r} - \left(\frac{\partial\mu_1}{\partial\rho^0}\right)_{p,T_{\mathrm{K}}}\frac{\partial\rho^0}{\partial r}\right\}, \tag{3}$$

where p is the pressure and T_{K} is the temperature in K. The pressure is given by

$$\partial p/\partial r = \rho\omega^2 r \tag{4}$$

so that eq. (3) can be rearranged to give

$$J_1^v = \left(\frac{\partial \mu_1}{\partial \rho^0}\right)_{p,T_K} K\left(\frac{1 - V_1\rho}{(\partial \mu_1/\partial \rho^0)_{p,T_K}}\omega^2 r - \frac{\partial \rho^0}{\partial r}\right), \tag{5}$$

where V_1 is the partial specific volume of the gradient-forming solute.

Diffusion coefficients reported in the literature are usually determined without rotation, at atmospheric pressure, and are defined by

$$J_1^{ex} = -D\,(\partial \rho_1^0/\partial r), \tag{6}$$

where D is the experimental diffusion coefficient, ρ_1^0 is the concentration in mass of solute per unit volume of solution at 1 atm, and the experimental flux J_1^{ex} is usually measured relative to a coordinate system attached to the apparatus. Eq. (6) can be written

$$J_1^{ex} = -\frac{D}{(\partial \rho^0/\partial \rho_1^0)_{p^0,T_K}}\frac{\partial \rho^0}{\partial r}, \tag{7}$$

where p^0 is the atmospheric pressure.

We now assume that the partial specific volumes of the solute, V_1, and solvent, V_2, are essentially constant. The partial specific volume of CsCl in water, for example, varies from about 0.24 cm^3/g i[illegible] · 28 cm^3/g in going from infinite dilution to saturation at 25°C. Under this assumption it can be shown [28] that the volume-mean velocity due to diffusion vanishes, so that $J_1^v = J_1^{ex}$. Comparing eqs. (5) and (7) for no rotation:

$$K = \frac{D}{(\partial \mu_1/\partial \rho^0)_{p,T}\,(\partial \rho/\partial \rho_1^0)_{p,T_K}}, \qquad \text{at 1 atm.} \tag{8}$$

At equilibrium in a centrifuge, the flux vanishes, and eq. (5) gives

$$\frac{\partial \rho^0}{\partial r} = \left(\frac{1 - V_1\rho}{(\partial \mu_1/\partial \rho^0)_{p,T_K}}\right)\omega^2 r. \tag{9}$$

The quantity in large parentheses in eq. (9) has been tabulated by a number of investigators [10,29] for various gradient-forming solutes, mainly at atmospheric pressure, and is denoted by Hearst et al. [29] by

$$\frac{1 - V_1\rho}{(\partial \mu_1/\partial \rho^0)_{p,T_K}} = \frac{1}{\beta(\rho^0, p)} = \frac{1 - \phi(p - p^0)}{\beta^0(\rho^0)}, \tag{10}$$

where $\beta^0(\rho^0)$ is the value of β at 1 atm, and $1 - \phi(p - p^0)$ is an approximate pressure correction.

We now introduce the approximation that the quantities K, D, β, and ρ can be evaluated at atmospheric pressure. The effect of pressure on β and ρ for CsCl solutions has been considered by Hearst et al. [29]. Based on their results, we estimate the maximum change of β due to pressure in the cases considered in this work to be several percent. If we ignore the pressure correction, eq. (5) becomes

$$J_1^v = \frac{D}{(\partial \rho^0/\partial \rho_1^0)_{p,T_K}}\left(\frac{\omega^2 r}{\beta^0(\rho^0)} - \frac{\partial \rho^0}{\partial r}\right). \tag{11}$$

The mass fluxes of components 1 and 2 are related by

$$V_1 J_1^v + V_2 J_2^v = 0. \tag{12}$$

The total mass flux J^v is given by

$$J^v = J_1^v + J_2^v = \left(1 - \frac{V_1}{V_2}\right) \frac{D}{(\partial \rho^0 / \partial \rho_1^0)_{p,T_K}} \left(\frac{\omega^2 r}{\beta^0(\rho^0)} - \frac{\partial \rho^0}{\partial r}\right). \tag{13}$$

The derivative in the denominator in eq. (13) can be obtained from

$$\rho_1 V_1 + \rho_2 V_2 = 1, \tag{14}$$

where ρ_2 is the concentration of the solvent, and

$$\rho = \rho_1 + \rho_2, \tag{15}$$

from which

$$\rho = \frac{1}{V_2} + \rho_1 \left(1 - \frac{V_1}{V_2}\right). \tag{16}$$

Since the partial specific volumes have been assumed constant, we have at atmospheric pressure

$$\left(\frac{\partial \rho^0}{\partial \rho_1^0}\right)_{p,T_K} = \left(1 - \frac{V_1}{V_2}\right), \tag{17}$$

so that

$$J^v = D\left(\frac{\omega^2 r}{\beta^0(\rho^0)} - \frac{\partial \rho^0}{\partial r}\right). \tag{18}$$

Since the volume-mean velocity due to diffusion vanishes for constant V_1, V_2, the law of conservation of mass becomes

$$\frac{\partial \rho}{\partial t} = -\frac{1}{r}\frac{\partial (r J^v)}{\partial r} = \frac{1}{r}\frac{\partial}{\partial r}\left\{rD\left(\frac{\partial \rho^0}{\partial r} - \frac{\omega^2 r}{\beta^0(\rho^0)}\right)\right\}. \tag{19}$$

We estimate the change of density at the outer periphery of the rotor due to a pressure change resulting from a complete gradient decay to be less than 1% of that due to composition changes of interest in the present work. Again using the approximation that the properties can be evaluated at 1 atm

$$\frac{\partial \rho^0}{\partial t} = \frac{1}{r}\frac{\partial}{\partial r}\left\{rD\left(\frac{\partial \rho^0}{\partial r} - \frac{\omega^2 r}{\beta^0(\rho^0)}\right)\right\}. \tag{20}$$

Assuming that the system is confined between nonpermeable concentric cylinders, the mass flux vanishes at both cylinders and we obtain as boundary conditions

$$\partial \rho^0 / \partial r = \omega^2 r / \beta^0(\rho^0), \qquad \text{at } r = r_{in}, r_{out}, \tag{21}$$

where r_{in}, r_{out} are the radii of the inner and outer cyclinders.

To solve eq. (20) numerically, we choose discrete values of the space and time variables by putting

$$r_j = r_{in} + (j - \tfrac{1}{2})(\Delta r), \qquad \Delta r = (r_{out} - r_{in})/(j_{max} - 2), \tag{22}$$

$$t^k = \sum_{l=1}^{k} (\Delta t^l), \tag{23}$$

where the spacial step Δr is constant and the time step Δt^l may be variable. We now replace the partial differential equation with the finite difference equation

$$\frac{\rho_j^{k+1} - \rho_j^k}{(\Delta t^{k+1})} = \tfrac{1}{2}\left(\frac{D_j^k}{r_j}\,\frac{r_{j+1/2}(\rho_{j+1}^{k+1} - \rho_j^{k+1}) - r_{j-1/2}(\rho_j^{k+1} - \rho_{j-1}^{k+1})}{(\Delta r)^2}\right.$$

$$+ \frac{D_j^k}{r_j}\,\frac{r_{j+1/2}(\rho_{j+1}^k - \rho_j^k) - r_{j-1/2}(\rho_j^k - \rho_{j-1}^k)}{(\Delta r)^2} + \frac{(D_{j+1}^k - D_{j-1}^k)(\rho_{j+1}^{k+1} - \rho_{j+1}^{k+1})}{(2\Delta r)^2}$$

$$\left. + \frac{(D_{j+1}^k - D_{j-1}^k)(\rho_{j+1}^k - \rho_{j-1}^k)}{(2\Delta r)^2}\right) - \frac{\omega^2}{r_j}\,\frac{(r_{j+1})^2 D_{j+1}^k/\beta_{j+1}^k - (r_{j-1})^2 D_{j-1}^k/\beta_{j-1}^k}{2\Delta r}, \tag{24}$$

where $\rho_j^k = \rho^0(t^k, r_j)$, etc.

The difference approximations used in eq. (12) are essentially those of Crank and Nicolson [30], but the diffusion coefficient and the quantity, β, both of which are known as a function of ρ^0, are evaluated at the "old" time, t^k, to avoid introducing terms which are nonlinear in the unknown ρ_j^{k+1}. As a result, the discretization error; that is, the error resulting from the replacement of eq. (20) by eq. (24), is second order in Δr but only first order in Δt^k. The boundary conditions, eq. (21), are also replaced by the difference expressions:

$$\frac{\rho_2^{k+1} - \rho_1^{k+1}}{\Delta r} = \tfrac{1}{2}\,\omega^2 r_{1.5}\left(\frac{1}{\beta_1^k} + \frac{1}{\beta_2^k}\right), \tag{25}$$

$$\frac{\rho_{j_{max}}^{k+1} - \rho_{j_{max}-1}^{k+1}}{\Delta r} = \tfrac{1}{2}\,\omega^2 r_{j_{max}-0.5}\left(\frac{1}{\beta_{j_{max}}^k} + \frac{1}{\beta_{j_{max}-1}^k}\right). \tag{26}$$

Any initial density distribution can be used. Given the density at the "old" time, t^k, eq. (24) was repeatedly solved for the density distribution at the "new" time, t^{k+1}, until the desired time interval was covered. The method of solution was that of Crank and Nicolson [30].

For small values of t, the density distribution may be nearly discontinuous and change rapidly with t, while for large values of t it is smoother and changes slowly. It was therefore decided to vary the time step, Δt^k, so as to use smaller steps initially. The variation in Δt^k was chosen so that

$$t^k = \alpha k^2. \tag{27}$$

It was found that when the value of α was too large, a numerical instability in the form of a bounded but persistent oscillation occurred.

A value of $\alpha = 0.0625\ (\Delta r)^2/D_{dil}$, where D_{dil} is the diffusivity of the gradient-forming solute at infinite dilution, was found to be satisfactory and did not lead to such oscillations.

The required value of the radial mesh size, Δr (or equivalently, the number of radial mesh points, j_{max}) depends on the accuracy required and on the smoothness of the initial density distribution. The most difficulty occurs with initial density distributions involving a step change in density, especially when the width of the step is a small frac-

tion of the radial gap of the centrifuge. Comparisons have been made between calculations with $j_{max} = 102$ and $j_{max} = 202$, using a step width of 10% of the radial gap in the initial density distribution. The comparison indicates that numerical discretization error with $j_{max} = 102$ is less than one part in 10^3 of the calculated density. If the initial density distribution had been smooth (e.g., parabolic) a smaller value of j_{max} could have been used. If the initial density distribution had involved a step width of only 1% of the radial gap, a larger value of j_{max} would have been needed to maintain the same accuracy.

2.2. A perturbation approximation for band behavior

In this section, a perturbation technique is applied to the Lamm equation for an arbitrary supporting gradient. The basis of the approximation is the assumption that the band of macromolecules is sufficiently narrow so that across the width of the band, the sedimentation velocity and diffusivity can be represented at any given time by polynomials of low degree in the radius. It is important to emphasize that the polynomial approximations need be valid only locally near the band, and that they may change as the band sediments through the gradient. Because the polynomials are permitted to change as the band moves, they can be of much lower degree than would be needed to represent the gradient globally.

Into the Lamm equation [31]

$$\frac{\partial c}{\partial t} = \frac{1}{r}\frac{\partial}{\partial r}\left[rD\frac{\partial c}{\partial r} - rvc\right], \tag{28}$$

where c is the concentration of macromolecules in the band, t is time, r is the radial distance from the axis of rotation, and the macromolecular diffusivity D and sedimentation velocity v are taken to be functions of r and t but not of c, we introduce the transformation

$$\zeta = [r - a(t)]\, b(t)/\epsilon, \tag{29}$$

$$C(\zeta, t) = a(t)\, b(t)\, c(r, t), \tag{30}$$

where the origin of the ζ-coordinate system $a(t)$ will be chosen to move along with the mean radius of the sedimenting band, and $b(t)$ is a reciprocal band width scaling function. Both $a(t)$ and $b(t)$ will be defined precisely later. The new concentration variable C has been modified to include radial dilution, and to include concentration changes which must accompany a change in band width. The constant ϵ has been introduced for convenience in the perturbation analysis. If b is of order unity, and ζ varies from -1 to $+1$ across the band, then the magnitude of ϵ is of the order of the band width, and ϵ will be considered a "small" parameter. The introduction of both $b(t)$ and ϵ as band width parameters is redundant since the value of ϵ can be incorporated into $b(t)$. This will be done after the perturbation analysis is carried out.

Transforming eq. (28):

$$\frac{\partial c}{\partial t} = D\frac{b^2}{\epsilon^2}\frac{\partial^2 C}{\partial \zeta^2} + \left\{\left(\frac{\partial D}{\partial r} + \frac{D}{r} - v\right)\frac{b}{\epsilon} + \dot{a}\frac{b}{\epsilon} + a\frac{\dot{b}}{\epsilon} - r\frac{\dot{b}}{\epsilon}\right\}\frac{\partial C}{\partial \zeta} + \left(-\frac{v}{r} - \frac{\partial v}{\partial r} + \frac{\dot{a}}{a} - \frac{\dot{b}}{b}\right)C, \tag{31}$$

where $\dot{a} = da/dt$ and $\dot{b} = db/dt$.

We now express v/r and D/r in Taylor series about the radius $a(t)$

$$v/r = \epsilon^{\sigma}\sum_{n=0}^{\infty} v_n\,[r - a(t)]^n = \sum_{n=0}^{\infty} v_n\,(\epsilon^{n+\sigma}/b^n)\,\zeta^n, \tag{32}$$

$$D/r = \epsilon^{\nu}\sum_{n=0}^{\infty} D_n\,[r - a(t)]^n = \sum_{n=0}^{\infty} D_n\,(\epsilon^{n+\nu}/b^n)\,\zeta^n, \tag{33}$$

where the coefficients v_n and D_n are understood to be functions of time, and the factors ϵ^σ and ϵ^ν are introduced for scaling purposes and will be discussed later. The expansions (32) and (33) need be valid only across the width of the band where the macromolecular concentration C differs significantly from zero. (Evidently, the band cannot include the axis of the centrifuge.) From eqs. (32) and (33) the following series can be obtained

$$v = \sum_{n=0}^{\infty} v_n (\epsilon^{n+1+\sigma}/b^{n+1}) \zeta^{n+1} + a \sum_{n=0}^{\infty} v_n (\epsilon^{n+\sigma}/b^n) \zeta^n, \tag{34}$$

$$\partial v/\partial r = \sum_{n=0}^{\infty} v_n (\epsilon^{n+\sigma}/b^n)(n+1)\zeta^n + a \sum_{n=0}^{\infty} n v_n (\epsilon^{n+\sigma-1}/b^{n-1}) \zeta^{n-1}, \tag{35}$$

$$D = \sum_{n=0}^{\infty} D_n (\epsilon^{n+1+\nu}/b^{n+1}) \zeta^{n+1} + a \sum_{n=0}^{\infty} D_n (\epsilon^{n+\nu}/b^n) \zeta^n, \tag{36}$$

$$\partial D/\partial r = \sum_{n=0}^{\infty} (n+1) D_n (\epsilon^{n+\nu}/b^n) \zeta^n + a \sum_{n=0}^{\infty} n D_n (\epsilon^{n+\nu-1}/b^{n-1}) \zeta^{n-1}. \tag{37}$$

The concentration is also expanded in a perturbation series

$$C(\zeta, t) = \sum_{n=0}^{\infty} \epsilon^n C_n(\zeta, t). \tag{38}$$

Substituting eqs. (32) through (38) into eq. (31), and rearranging the summations to collect powers of ϵ,

$$\begin{aligned}
\sum_{l=0}^{\infty} \epsilon^l \partial C_l/\partial t = {} & \sum_{l=\nu-1}^{\infty} \epsilon^l \sum_{n=0}^{l+1-\nu} D_n b^{1-n} \zeta^{n+1} \partial^2 C_{l+1-\nu-n}/\partial\zeta^2 \\
& + a \sum_{l=\nu-2}^{\infty} \epsilon^l \sum_{n=0}^{l+2-\nu} D_n b^{2-n} \zeta^n \partial^2 C_{l+2-\nu-n}/\partial\zeta^2 + \sum_{l=\nu-1}^{\infty} \epsilon^l \sum_{n=0}^{l+1-\nu} (n+2) D_n b^{1-n} \zeta^n \partial C_{l+1-\nu-n}/\partial\zeta \\
& + a \sum_{l=\nu-2}^{\infty} \epsilon^l \sum_{n=0}^{l-\nu+2} n D_n b^{2-n} \zeta^{n-1} \partial C_{l-\nu+2-1}/\partial\zeta - \sum_{l=\sigma}^{\infty} \epsilon^l \sum_{n=0}^{l-\beta} V_n b^{-n} \zeta^{n+1} \partial C_{l-\sigma-n}/\partial\zeta \\
& - a \sum_{l=\sigma-1}^{\infty} \epsilon^l \sum_{n=0}^{l+1-\sigma} v_n b^{1-n} \zeta^n \partial C_{l+1-\sigma-n}/\partial\zeta + \sum_{l=-1}^{\infty} \epsilon^l \dot{a} b \partial C_{l+1}/\partial\zeta - \sum_{l=0}^{\infty} \epsilon^l \dot{b} b^{-1} \zeta \partial C_l/\partial\zeta \\
& - \sum_{l=\sigma}^{\infty} \epsilon^l \sum_{n=0}^{l-\sigma} (n+2) v_n b^{-n} \zeta^n C_{l-\sigma-n} - a \sum_{l=\sigma-1}^{\infty} \epsilon^l \sum_{n=0}^{l-\sigma+1} n v_n b^{1-n} \zeta^{n-1} C_{l+1-\sigma-n} \\
& + \sum_{l=0}^{\infty} \epsilon^l (a^{-1}\dot{a} - b^{-1}\dot{b}) C_l.
\end{aligned} \tag{39}$$

There are physically attainable situations in which the propagation of a band is governed almost entirely by diffusion with only a slight correction due to sedimentation, and vice versa. Corresponding to these situations it

is possible, by appropriate choice of the scaling parameters ν and σ, to obtain equations for C_l in which the sedimentation affects only the higher order perturbations and not the dominant term C_0, etc. In the present work, the objective is to include both diffusion and sedimentation in the dominant term C_0. This is achieved by the choice $\nu = 1$, $\sigma = 0$. Then, equating the coefficients of ϵ^{-1} in eq. (39)

$$(-av_0 b + \dot{a}b)\,\partial C_0/\partial\zeta = 0. \tag{40}$$

Eq. (40) is satisfied by choosing

$$\dot{a} = av_0 \tag{41}$$

with $a(0)$ equal to the mean starting radius of the band, which causes the origin of the ζ-coordinate system to translate along with a sedimenting particle.

Equating the coefficients of ϵ^l, $l \geqslant 0$ and using eq. (41)

$$\frac{\partial C_l}{\partial t} - ab^2 D_0 \frac{\partial^2 C_l}{\partial \zeta^2} + [b^{-1}\dot{b} + v_0 + av_1]\,\zeta \frac{\partial C_l}{\partial \zeta} + [b^{-1}\dot{b} + v_0 + av_1]\,C_l = \sum_{n=1}^{l} \left\{ (D_{n-1} + AD_n)\, b^{2-n} \zeta^n \frac{\partial^2 C_{l-n}}{\partial \zeta^2} \right.$$

$$+ [(n+1)\,D_{n-1} + AD_n\, b^{2-n}\, \zeta^{n-1} - (v_n + av_{n+1})\, b^{-n}\, \zeta^{n+1}] \frac{\partial C_{l-n}}{\partial \zeta}$$

$$\left. + [-(n+2)v_n - (n+1)av_{n+1}]\, b^{-n} \zeta^n C_{l-n} \right\}. \tag{42}$$

Eq. (42) determines the concentration perturbation C_l. It is to be solved sequentially for the values of l of interest, starting with $l = 0$. Then the right-hand side of eq. (42) is always a known function. For $l = 0$ the right-hand side vanishes. The band width scaling function $b(t)$ is still undefined and can be chosen in various ways to simplify eq. (42).

Initial and boundary conditions are needed for eq. (42). At $t = 0$, the starting concentration profile may be represented exactly (or to the desired degree of precision) by the first term in the perturbation series, so that

$$C_0(\zeta, 0) = a(0)\, b(0)\, c(r, 0), \tag{43}$$

$$C_l(\zeta) = 0, \qquad l \geqslant 1. \tag{44}$$

To provide boundary conditions, the band is assumed to be localized so that the macromolecular concentration becomes negligible before a wall of the centrifuge is reached. The ζ-coordinate system is then extended to $\pm\infty$, and

$$C_l(\zeta, t) \to 0 \quad \text{as} \quad \zeta \to \pm\infty,\ l \geqslant 0. \tag{45}$$

For numerical calculations to be presented later in this paper, the following equations for v, D were used:

$$v = S_{20,w}\, \omega^2 r \left(\frac{1 - V_m \rho}{1 - V_m \rho_{20,w}} \right) \frac{\eta_{20,w}}{\eta}, \tag{46}$$

where ω is the angular velocity of the centrifuge, V_m is the partial specific volume of the macromolecule, ρ, η are the local instantaneous density and viscosity of the gradient solution, $\rho_{20,w}$, $\eta_{20,w}$ are the density and viscosity of water at 20°C, and $S_{20,w}$ is the sedimentation velocity in water at 20°C and unit acceleration. The gradient properties ρ, η are functions of r, t. Variations in V_m have not been considered. Viscosity and temperature corrections were applied to the diffusivity:

$$D = D_{20,w} \left(\frac{T_K}{293} \right) \frac{\eta_{20,w}}{\eta}, \tag{47}$$

where T_K is the temperature in kelvin and $D_{20,w}$ is the diffusivity in water at 20°C.

The perturbation parameter ϵ of eq. (38) is no longer needed and will be set equal to one for the remainder of this work.

2.3. An error function solution

Several methods of obtaining solutions to eq. (42) have been investigated. In this section, solutions in terms of repeated integrals of the error function are considered.

We define $b(t)$ by the differential equation

$$\dot{b} = -bv_0 - bav_1 \tag{48}$$

with $b(0)$ equal to the reciprocal of the starting band width, and also introduce a new time variable T defined by

$$\dot{T} = ab^2 D_0. \tag{49}$$

Then eq. (42) becomes

$$\frac{\partial C_l}{\partial T} - \frac{\partial^2 C_l}{\partial \xi^2} = \frac{1}{ab^2 D_0} \sum_{n=1}^{l} \left\{ (D_{n-1} + aD_n) \frac{\xi^n}{b^{n-2}} \frac{\partial^2 C_{l-n}}{\partial \xi^2} + \left([(n+1)D_{n-1} + anD_n] \frac{\xi^{n-1}}{b^{n-2}} - (v_n + av_{n+1}) \frac{\xi^{n+1}}{b^n} \right) \frac{\partial C_{l-n}}{\partial \xi} + [-(n+2)v_n - (n+1)av_{n+1}] \frac{\xi^n}{b^n} C_{l-n} \right\}. \tag{50}$$

The starting concentration profile is most conveniently idealized by a rectangular shape

$$\begin{aligned} c(r, 0) &= 0, && r < a_0 - w/2, \\ &= c^0, && a_0 - w/2 < r < a_0 + w/2, \\ &= 0, && a_0 + w/2 < r. \end{aligned} \tag{51}$$

or a triangular shape such as used, for example, by Eikenberry et al. [32]

$$\begin{aligned} c(r, 0) &= 0, && r < a_0 - w/3, \\ &= [\tfrac{2}{3} - (r - a_0)/w]\, c^0, && a_0 - w/3 < r < a_0 + 2w/3, \\ &= 0, && a_0 + 2w/3 < r, \end{aligned} \tag{52}$$

where w is the starting band width, $a_0 = a(0)$ is the band center starting radius, and c_0 is the maximum starting concentration. [In eq. (52), the band center radius a_0 has been chosen to be the radius of the centroid of the triangle.] We consider a generalization of these profiles in which the starting concentration is assumed to be represented by a piecewise polynomial function, i.e., the profile is made up of a finite number of segments, with a different polynomial concentration distribution in each segment. Such a function can be written as a finite sum of the form

$$c(r, 0) = \sum_{j=1}^{J} \alpha_j R_{k_j} (r - a_0 - \xi_j), \tag{53}$$

where α_j, k_j and ξ_j are constants (k_j a nonnegative integer), and R_k is a generalized ramp function defined by

$$R_k(x) = (-x)^k, \qquad x < 0,$$
$$= 0, \qquad x > 0, \tag{54}$$

For example, the triangular band given in eq. (52) can be written in terms of ramp functions as

$$c(r, 0) = \frac{c^0}{w} R_1(r - a_0 - 2w/3) - \frac{c^0}{w} R_1(r - a_0 + w/3) - c_0 R_0(r - a_0 + w/3). \tag{55}$$

The initial condition for C_0 corresponding to eq. (53) is

$$C_0(\xi, 0) = a(0)\, b(0) \sum_{j=1}^{J} \alpha_j R_{k_j}[\xi/b(0) - \xi_j] = a(0)\, b(0) \sum_{j=1}^{J} \alpha_j [b(0)]^{-k_j} R_{k_j}[\xi - \xi_j b(0)]. \tag{56, 57}$$

For the case $l = 0$, eq. (50) reduces to the diffusion equation

$$\partial C_0/\partial T = \partial^2 C_0/\partial \xi^2. \tag{58}$$

Since eq. (58) is linear it can be solved for the initial condition eq. (57) term by term. The solution of eq. (58) satisfying the initial condition for a typical term of the form

$$C_0(\xi, 0) = R_k(\xi - \xi) \tag{59}$$

is given by (as may be verified by direct substitution)

$$C_0(\xi, T) = \tfrac{1}{2}\, k!\, (4T)^{k/2}\, \mathrm{i}^k \operatorname{erfc}\left(\frac{\xi - \xi}{4T}\right), \tag{60}$$

where $\mathrm{i}^k \operatorname{erfc}(x)$ is the kth repeated integral of the complementary error function, i.e.,

$$\mathrm{i}^{-1} \operatorname{erfc}(x) = (2/\sqrt{\pi}) \exp(-x^2), \tag{61}$$

$$\mathrm{i}^0 \operatorname{erfc}(x) = \operatorname{erfc}(x) = \int_x^\infty (2/\sqrt{\pi}) \exp(-y^2)\, dy, \qquad k \geqslant 0, \tag{62}$$

$$\mathrm{i}^k \operatorname{erfc}(x) = \int_x^\infty \mathrm{i}^{k-1} \operatorname{erfc}(y)\, dy, \qquad k \geqslant 0. \tag{63}$$

Tables and some properties of the function $\mathrm{i}^k \operatorname{erfc}(x)$ are given by Abramowitz and Stegun [33]. One property which will be needed later is the recurrence relation

$$k\mathrm{i}^k \operatorname{erfc}(x) = -x\, k^{i-1} \operatorname{erfc}(x) + \tfrac{1}{2}\, \mathrm{i}^{k-2} \operatorname{erfc}(x), \tag{64}$$

which can also be applied repeatedly to evaluate $\mathrm{i}^k \operatorname{erfc}(x)$ by starting with eqs. (61) and (62).

The solution of eq. (58) for the initial condition eq. (57) is then given by

$$C_0(\xi, T) = a(0)\, b(0) \sum_{j=1}^{J} \alpha_j \tfrac{1}{2} (k_j)!\, [b(0)]^{-k_j} [4T]^{k_j/2} \mathrm{i}^{k_j} \operatorname{erfc}\{[(r - a)\, b - \xi_j b(0)]/\sqrt{4T}\}, \tag{65}$$

where a, b, and T are functions of time defined by the ordinary differential eqs. (41), (48) and (49). Eq. (65) satisfies the boundary conditions eq. (45) provided the initial concentration satisfies those conditions.

Eq. (65) gives the lowest order term of the perturbation series. To find the next higher order correction, we put $l = 1$ in eq. (50)

$$\frac{\partial C_1}{\partial T} - \frac{\partial^2 C_1}{\partial \zeta^2} = \frac{1}{ab^2 D_0}\left((D_0 + aD_1)b\zeta \frac{\partial^2 C_0}{\partial \zeta^2} + [(2D_0 + aD_1)b - (v_1 + av_2)b^{-1}\zeta^2]\frac{\partial C_0}{\partial \zeta}\right.$$

$$\left. + (-3v_1 - 2av_2)\, b^{-1}\zeta C_0\right). \tag{66}$$

Eq. (65) for C_0 can now be substituted into eq. (66) to evaluate the right-hand side. The substitution involves differentiation with respect to ζ, and multiplication by a power of ζ. The derivative of the function i^k erfc can be obtained by differentiating eq. (63)

$$\mathrm{i}^{k-1}\,\mathrm{erfc}(x) = -\frac{\mathrm{d}}{\mathrm{d}x}\,[\mathrm{i}^k\,\mathrm{erfc}(x)], \qquad k \geqslant 0, \tag{67}$$

however, values of k less than minus one can occur, so it is convenient to extend the definition of i^k erfc to arbitrary negative values of k by using eq. (67) as the definition, starting at $k = 0$. The resulting functions can be expressed in terms of Hermite polynomials and will be referred to again in the next section. The recurrence relation eq. (64) remains valid for arbitrary negative values of k. Eq. (67) makes it possible to express the derivatives occurring in eq. (66) in terms of the function i^k erfc multiplied by some function of time. By using eq. (64), the same can be done for multiplication by ζ, for example, for a typical term

$$\zeta \mathrm{i}^k\,\mathrm{erfc}\left(\frac{\zeta - \xi b(0)}{\sqrt{4T}}\right) = \sqrt{4T}\left(\frac{\zeta - \xi b(0)}{\sqrt{4T}}\right)\mathrm{i}^k\,\mathrm{erfc}\left(\frac{\zeta - \xi b(0)}{\sqrt{4T}}\right) + \xi\, b(0)\,\mathrm{i}^k\,\mathrm{erfc}\left(\frac{\zeta - \xi b(0)}{\sqrt{4T}}\right)$$

$$= (k+1)\sqrt{4T}\,\mathrm{i}^{k+1}\,\mathrm{erfc}\left(\frac{\zeta - \xi b(0)}{\sqrt{4T}}\right) + \tfrac{1}{2}\sqrt{4T}\,\mathrm{i}^{k-1}\,\mathrm{erfc}\left(\frac{\zeta - \xi b(0)}{\sqrt{4T}}\right) + \xi\, b(0)\,\mathrm{i}^k\,\mathrm{erfc}\left(\frac{\zeta - \xi b(0)}{\sqrt{4T}}\right). \tag{68}$$

The right-hand size of eq. (66) can then be expressed as a series of terms each of the form

$$f(T)\,\mathrm{i}^k\,\mathrm{erfc}\left(\frac{\zeta - \xi b(0)}{\sqrt{4T}}\right), \tag{69}$$

where $f(T)$ is some function of T.

Since eq. (66) is linear it can be solved term by term. The typical equation

$$\frac{\partial C_1}{\partial T} - \frac{\partial^2 C_1}{\partial \zeta^2} = f(T)\,\mathrm{i}^k\,\mathrm{erfc}\left(\frac{\zeta - \xi b(0)}{\sqrt{4T}}\right) \tag{70}$$

has a solution (as may be verified by direct substitution)

$$C_1(\zeta, T) = g(T)\,\mathrm{i}^k\,\mathrm{erfc}\left(\frac{\zeta - \xi b(0)}{\sqrt{4T}}\right), \tag{71}$$

where $g(T)$ is given by the ordinary differential equation

$$\frac{\mathrm{d}g}{\mathrm{d}T} - \frac{k}{2T}\,g = f(T), \qquad \text{with } g(0) = 0. \tag{72}$$

The solution of eq. (72) is

$$g(T) = T^{k/2}\int_0^T T^{-k/2} f(T)\,\mathrm{d}T. \tag{73}$$

A detailed examination of the integrals needed for a complete solution of eq. (66) reveals that, regardless of the number of terms of the series of eq. (65), at most eight integrals of the type in eq. (73) are needed. They are

$$I_1(T) = \int_0^T \frac{b(D_0 + aD_1)}{ab^2D_0}\,dT, \qquad I_2(T) = \int_0^T \frac{b(D_0 + aD_1)}{ab^2D_0}\,T\,dT, \qquad I_3(T) = \int_0^T \frac{b(2D_0 + aD_i)}{ab^2D_0}\,dT,$$

$$I_4(T) = \int_0^T \frac{v_1 + av_2}{bab^2D_0}\,dT, \qquad I_5(T) = \int_0^T \frac{v_1 + av_2}{bab^2D_0}\,T\,dT, \qquad I_6(T) = \int_0^T \frac{v_1 + av_2}{bab^2D_0}\,T^2\,dT$$

$$I_7(T) = \int_0^T \frac{3v_1 + 2av_2}{bab^2D_0}\,dT, \qquad I_8(T) = \int_0^T \frac{3v_1 + 2av_2}{bab^2D_0}\,T\,dT, \tag{74}$$

In terms of the integrals given above, the complete solution of eq. (66) is

$$C_1(\xi, T) = a(0)\,b(0) \sum_{j=1}^{J} \alpha_j\,[b(0)]^{-k_j}\,\tfrac{1}{2}(k_j)!\,\Bigg\{[k_j(k_j+1)I_4 + (k_j+1)I_7]\,(4T)^{(k_j+1)/2}$$

$$\times\, i^{k_j+1}\,\operatorname{erfc}\left(\frac{\xi - \xi_j b(0)}{\sqrt{4T}}\right) + [-2k_j\xi_j b(0)I_4 - \xi_j b(0)I_7]\,(4T)^{k_j/2}\,i^{k_j}\operatorname{erfc}\left(\frac{\xi - \xi_j b(0)}{\sqrt{4T}}\right)$$

$$+ [(-k_j+1)I_1 - I_3 + (-4k_j+2)I_5 + \xi_j^2 b^2(0)I_4 - 2I_8]\,(4T)^{(k_j-1)/2}\,i^{k_j-1}\operatorname{erfc}\left(\frac{\xi - \xi_j b(0)}{\sqrt{4T}}\right)$$

$$+ [\xi_j b(0)I_1 + 4\xi_j b(0)I_5]\,(4T)^{(k_j-2)/2}\,i^{k_j-2}\operatorname{erfc}\left(\frac{\xi - \xi_j b(0)}{\sqrt{4T}}\right)$$

$$+ (2I_2 + 4I_6)\,(4T)^{(k_j-3)/2}\,i^{k_j-3}\operatorname{erfc}\left(\frac{\xi - \xi_j b(0)}{\sqrt{4T}}\right)\Bigg\}. \tag{75}$$

The same procedure used above to obtain C_1 can be carried out to obtain C_l for higher values of l, but the complexity of the solutions grows rapidly, and the process will not be carried further here. With the zeroth and first order perturbation, the concentration becomes

$$c(r, t) = \frac{1}{a(t)\,b(t)}\,[C_0(\xi, T) + C_1(\xi, T)]. \tag{76}$$

2.4. An eigenfunction solution

In this section an alternative method of solution for eq. (42) is presented in the form of an infinite series of eigenfunctions.

If the band width scaling function $b(t)$ is defined by the differential equation

$$\dot{b} = -b(v_0 + av_1 + 2ab^2D_0) \tag{77}$$

and the new time variable is again defined by

$$\dot{T} = ab^2D_0 \tag{78}$$

eq. (42) takes the form

$$\frac{\partial C_l}{\partial T} - \frac{\partial^2 C_l}{\partial \xi^2} - 2\xi \frac{\partial C_l}{\partial \xi} - 2C_l = \frac{1}{ab^2 D_0} \sum_{n=1}^{l} \left\{ (D_{n-1} + aD_n) b^{2-n} \xi^n \frac{\partial^2 C_{l-n}}{\partial \xi^2} \right.$$

$$+ \{ [(n+1) D_{n-1} + anD_n] b^{2-n} \xi^{n-1} - (v_n + av_{n+1}) b^{-n} \xi^{n+1} \} \frac{\partial C_{l-n}}{\partial \xi}$$

$$\left. - [(n+2) v_n - (n+1) v_{n+1}] b^{-n} \xi^n C_{l-n} \right\}. \tag{79}$$

For the case $l = 0$, when the right-hand side banishes, eq. (79) can be solved by separation of variables. The solution obtained is of the form

$$C_0(\xi, T) = \sum_{m=0}^{\infty} A_{0m}(T) \psi_m(\xi), \tag{80}$$

where

$$\psi_m(\xi) = \frac{1}{\sqrt{\sqrt{\pi}\, 2^m m!}} (-1)^m \frac{d^m}{d\xi^m} (e^{-\xi^2}) = \frac{e^{-\xi^2}}{\sqrt{\sqrt{\pi}\, 2^m m!}} H_m(\xi). \tag{81}$$

$H_m(\xi)$ is the Hermite polynomial of order m

$$A_{0m}(T) = A_{0m}(0)\, e^{-2mT}. \tag{82}$$

$A_{0m}(0)$ is the coefficient of the expansion of the starting concentration $C_0(\xi, 0)$ in terms of the functions $\psi_m(\xi)$.

The denominator of eq. (81) is the usual normalization factor for Hermite functions. To avoid the repeated appearance of this factor in later equations, we define

$$h_m(\xi) = \frac{1}{\sqrt{\sqrt{\pi}\, 2^m m!}} H_m(\xi). \tag{83}$$

The functions $\psi_m(\xi)$ satisfy the weighted orthogonality condition

$$\int_{-\infty}^{\infty} e^{\xi^2} \psi_m(\xi) \psi_n(\xi)\, d\xi = 0, \qquad m \neq n,$$
$$= 1, \qquad n = m, \tag{84}$$

so that the series expansion coefficients can be obtained from the equation

$$A_{0m}(0) = \int_{-\infty}^{\infty} e^{\xi^2} \psi_m(\xi) C_0(\xi, 0)\, d\xi. \tag{85}$$

Numerical experiments, however, indicate that the use of a truncated series obtained in this way is not a very efficient method of representing a function. For example, for the function

$$f(\xi) = 0, \quad \xi < -\xi_0$$
$$= 1, \quad -\xi_0 \leq \xi \leq \xi_0$$
$$= 0, \quad \xi_0 < \xi \tag{86}$$

the series expansion is satisfactory for ζ_0 on the order of unity or less, but when ζ_0 is larger, the Gibbs oscillations which originate at the discontinuities tend to be amplified strongly near $\zeta = 0$, in some cases becoming orders of magnitude greater than the function itself. This difficulty appears to result from the weighting function e^{ζ^2} in eq. (84), which greatly emphasizes large values of ζ at the expense of the range near $\zeta = 0$.

To obtain a more efficient truncated series expansion, the following indirect method has been used. A new variable

$$Z = \sqrt{2}\,\zeta \tag{87}$$

is introduced, and the initial concentration is expanded in a series of Hermite orthogonal functions

$$C_0(Z/2, 0) = \sum_{m=0}^{\infty} B_m \Phi_m(Z), \qquad \text{where } \Phi_m(Z) = e^{-Z^2/2} h_m(Z). \tag{88}$$

The functions $\Phi_m(Z)$ satisfy the unweighted orthogonality relation

$$\begin{aligned} \int_{-\infty}^{\infty} \Phi_m(Z)\,\Phi_n(Z)\,dZ &= 0, \qquad m \neq n, \\ &= 1, \qquad n = m, \end{aligned} \tag{89}$$

so that difficulties associated with a wide variation in weight are avoided, and

$$B_m = \int_{-\infty}^{\infty} \Phi_m(Z)\, C_0\,(Z/\sqrt{2}, 0)\, dZ. \tag{90}$$

A truncated series of the form of eq. (88) can then be written in terms of ζ as

$$C_0(\zeta, 0) \approx \sum_{m=0}^{M} B_m e^{-\zeta^2} h_m(\sqrt{2}\,\zeta) \tag{91}$$

The right-hand side of eq. (91) has the form of $e^{-\zeta^2}$ times a polynomial in ζ of degree M. Any such function can be written exactly in the form

$$\sum_{m=0}^{M} B_m e^{-\zeta^2} h_m(\sqrt{2}\,\zeta) = \sum_{m=0}^{M} A_{0m}(0)\, e^{-\zeta^2} n_m(\zeta) = \sum_{m=0}^{M} A_{0m}(0)\, \psi_m(\zeta). \tag{92}$$

Thus the truncated expansion in Hermite orthogonal functions, eq. (91) can be rearranged without further approximation into the desired form of eq. (92). The rearrangement is most conveniently carried out by making use of the orthogonality properties and the integral result

$$\begin{aligned} K_{m,n}(u) = \int_{-\infty}^{+\infty} \sum h_m(\zeta)\, h_n(u\zeta)\, e^{-\zeta^2}\, d\zeta \; &= \frac{(2u)^m\,(u-1)^{(n-m)/2}}{2^{(n+m)/2}\,[(n-m)/2]\,!} \left(\frac{n!}{m!}\right)^{1/2}, \qquad \text{if } n \geqslant m \text{ and } (n-m) \text{ is even,} \\ &= 0, \qquad \text{otherwise,} \end{aligned} \tag{93}$$

which can be obtained from the contour integral representation of the Hermite polynomials [33]. The coefficients $A_{0m}(0)$ and B_m are then related by

$$A_{0m}(0) = \sum_{n=0}^{m} K_{mn}(\sqrt{2})\, B_n. \tag{94}$$

Eq. (80) then gives the eigenfunction form of the solution for $C_0(\xi, T)$.

For higher order perturbations we seek a solution of the same form

$$C_l(\xi, T) = \sum_{m=0}^{\infty} A_{lm}(T)\, \psi_m(\xi), \tag{95}$$

where $\psi_m(\xi)$ is again given by eq. (64), but $A_{lm}(T)$ is now an arbitrary function of T, not necessarily of the form of eq. (82). An ordinary differential equation for $A_{lm}(T)$ can be obtained, making use of the orthogonality of the $\psi_m(\xi)$, by substituting eq. (95) into eq. (79), multiplying by

$$e^{\xi^2}\, \psi_k(\xi) = h_k(\xi) \tag{96}$$

and integrating from $-\infty$ to ∞. After some integration by parts the following equation is obtained

$$\frac{dA_{lk}}{dT} + 2\,kA_{lk} = \sum_{n=1}^{l} \{b^{2-n}[D_{n-1} + aD_n]\, D_n^2\, \phi_k^n - b^{2-n}[(n+1)D_{n-1} + anD_n]\, D_k \phi_k^{n-1}$$

$$+ b^{-n}(v_n + av_{n+1})\, D_k\, \phi_k^{n+1} - b^{-n}\,[(n+2)v_n + (n+1)av_{n+1}]\, \dot{\phi}_k^n\}\, A_{l-n,k}, \tag{97}$$

where ϕ_k and D_k are operators, which act on a sequence of expansion coefficients, defined by

$$\phi_k V_k = \sqrt{(k+1)/2}\, V_{k+1} + \sqrt{k/2}\, V_{k-1}, \qquad D_k V_k = \sqrt{2k}\, V_{k-1}, \tag{98,99}$$

and superscripts on ϕ_n or D_n indicate repeated application of the operator. Eq. (98) is based on the recurrence relation for normalized Hermite polynomials

$$\xi\, h_k(\xi) = \sqrt{(k+1)/2}\, h_{k+1}(\xi) + \sqrt{k/2}\, h_k(\xi) \tag{100}$$

and ϕ_k is simply the operator which, when applied to the series expansion coefficients, corresponds to multiplying the series by ξ. Similarly D_k is the differentiation operator based on

$$\frac{dh_k(\xi)}{d\xi} = \sqrt{2k}\, h_{k-1}(\xi). \tag{101}$$

To match the initial condition eq. (44) we have

$$A_{lk}(0) = 0 \qquad \text{for } l \geqslant 1. \tag{102}$$

If the zeroth-order series is truncated at M terms so that

$$A_{0k} = 0, \qquad \text{for } k > M \text{ and } T \geqslant 0, \tag{103}$$

then it follows from eq. (97) that

$$A_{1k} = 0, \qquad \text{for } k > M + 3 \text{ and } T \geqslant 0, \tag{104}$$

$$A_{2k} = 0, \qquad \text{for } k > M + 7 \text{ and } T \geqslant 0, \tag{105}$$

etc. That is, each of the higher order series involves only a finite number of terms, and no further truncation need be carried out. This is useful because of the difficulties associated with truncation discussed earlier.

Eq. (97) involves one ordinary differential equation for each non-zero term of the series eq. (95). For the case $l = 1$, the solution of these equations can be reduced to at most eight integrations by the substitution

$$A_{1m}(T) = Y_{1m}(T)\,e^{-2mT}, \qquad A_{0m}(T) = Y_{0m}(T)\,e^{-2mT}. \tag{106}$$

For $l = 1$, eq. (97) then reduces to

$$\begin{aligned}\frac{dy_{1m}}{dT} = \frac{1}{ab^2D_0}\,&\{[(m+2)\sqrt{(m+1)/2}\,b^{-1}(v_1 + av_2)\,e^{-2T} - \sqrt{(m+1)/2}\,b^{-1}(3v_1 + 2av_2)\,e^{-2T}]\,Y_{0,m+1}\\ &+ [(m+1)\sqrt{2m}\,b(D_0 + aD_1)e^{2T} - \sqrt{2m}\,b(2D_0 + aD_1)e^{2T} + (2m+1)\sqrt{m/2}\,b^{-1}(v_1 + av_2)e^{2T}\\ &- \sqrt{m/2}\,b^{-1}(3v_1 + 2av_2)e^{2T}]\,Y_{0,m-1}\\ &+ [\sqrt{2m(m-1)(m-2)}\,b(D_0 + aD_1)\,e^{6T} + \sqrt{m(m-1)(m-2)/2}\,b^{-1}(v_1 + av_2)e^{6T}]\,Y_{0,m-3}\}.\end{aligned} \tag{107}$$

Eq. (107) can be integrated directly and, in view of eq. (82), the quantities $Y_{0,m}$ are all constants. The eight integrals needed are

$$J_1(T) = \int_0^T \frac{b(D_0 + aD_1)}{ab^2D_0}\,e^{2T}dT, \qquad J_2(T) = \int_0^T \frac{b(D_0 + aD_1)}{ab^2D_0}e^{6T}dT, \qquad J_3(T) = \int_0^T \frac{b(2D_0 + aD_1)}{ab^2D_0}\,e^{2T}dT,$$

$$J_4(T) = \int_0^T \frac{v_1 + av_2}{bab^2D_0}\,e^{-2T}dT, \qquad J_5(T) = \int_0^T \frac{v_1 + av_2}{bab^2D_0}e^{2T}dT, \qquad J_6(T) = \int_0^T \frac{v_1 + av_2}{bab^2D_0}\,e^{6T}dT,$$

$$J_7(T) = \int_0^T \frac{3v_1 + 2av_2}{bab^2D_0}\,e^{-2T}dT, \qquad J_8(T) = \int_0^T \frac{3v_1 + 2av_2}{bab^2D_0}\,e^{2T}dT. \tag{108}$$

In terms of the above integrals, the solution of eq. (79) for $l = 1$ is

$$\begin{aligned}C_1(\xi, T) = \sum_{m=0}^{\infty}\,&\{[(m+2)\sqrt{(m+1)/2}\,J_4 - \sqrt{(m+1)/2}\,J_7]\,A_{0,m+1}(0)\\ &+ [(m+1)\sqrt{2m}\,J_1 - \sqrt{2m}\,J_3 + (2m+1)\sqrt{m/2}\,J_5 - \sqrt{m/2}\,J_8]\,A_{0,m-1}(0)\\ &+ [\sqrt{2m(m-1)(m-2)}\,J_2 + \sqrt{m(m-1)(m-2)/2}\,J_6]\,A_{0,m-3}(0)\}\,e^{-2mT}e^{-\xi^2}h_m(\xi).\end{aligned} \tag{109}$$

The above processes can be applied to higher values of l, but will not be carried further here.

When the gradient concentration profile is known as a function of radius and time, the determination of the radius of the band center requires the evaluation of one integral to solve eq. (41). If two additional integrals are evaluated [to solve eqs. (48) and (49) or eqs. (77) and (78)], the zeroth approximation to the band shape can be calculated. If eight additional integrals are evaluated, the $l = 1$ approximation can be calculated.

In some simple cases, the equations can be solved or the integrals evaluated analytically. This can be done, for

example, in the case considered by Schumaker [34] and by Baldwin and Schooter [19]. They let

$$v = E + Fr, \qquad D = G,$$

where E, F, G are constants.

Then the solution of eqs. (41), (48), (49) becomes

$$a(t) = [a(0) + E/F]\ e^{Ft} - E/F, \tag{110}$$

$$b(t) = b(0)\ e^{-Ft}, \tag{111}$$

$$T(t) = -[Gb^2(0)/2F]\ (e^{-2Ft} - 1). \tag{112}$$

Eqs. (110), (111), (112) can be substituted into eq. (65) to obtain the zeroth approximation to the band shape for any starting band. Eq. (74) can also be evaluated analytically in this case to obtain the first order approximation.

In complicated cases where the gradient must be evaluated numerically, numerical evaluation of the integrals needed for a band calculation is also necessary. A computer program has therefore been written to calculate the evolution of the gradient according to eq. (24), and at the same time, to evaluate the integrals needed to determine the band propagation. The program uses eq. (65) for the zeroth approximation and eq. (109) for the first order approximation.

2.5. Gradient solution properties

Calculation of the transient diffusion and sedimentation of the gradient-forming solute as described above requires that the diffusivity and β^0 be known at every concentration in the centrifuge. Calculation of the sedimentation of a particle requires knowledge of the viscosity and density of the gradient-forming solution. All of the above quantities depend on the composition of the gradient-forming solution, which we characterize in this section by the mass fraction W (grams of gradient-forming solute per gram of solution). To describe a solute, four functions must be defined:

$$W(\rho, T),\ D(W, T),\ \beta(W, T), \text{ and } \eta(W, T)$$

In most cases these functions have been obtained by fitting a polynomial or other simple function by the method of least squares, to data found in the literature. The accuracy of the data is usually not definitely known, and varies widely from property and from investigator to investigator. To give some indication of the error involved, the standard deviation of the data from the least-squares function is given in table 2. Certainly the accuracy of the present functions is no better than the reported standard deviation, and it could be much worse if the data were smoothed by the original investigator, or if they contain some systematic (non-random) error.

Six gradient-forming solutes are considered: CsCl, sucrose, KBr, NaBr, K_2 tartrate, and K_3 citrate. For the last four solutes, properties have been correlated only at 25°C. Since it is sometimes necessary to carry out centrifugation below room temperature, properties of CsCl and sucrose have been correlated as a function of temperature as well as concentration, and are considered usable (with some loss of accuracy) over a range of approximately $30°C \geq T \geq 0°C$.

In the present work, it was decided that the effect of pressure on the above properties could be neglected without an unacceptable error, and only properties at 1 atm have been considered. Some indication of the effect of pressure is available from the work of Hearst et al. [29].

Since the mass fraction was adopted as a measure of concentration in the correlation of properties, the definition of β^0 was used in the form:

$$\beta^0 = \frac{2RT_K V^3}{M}\left\{\frac{1}{W(1-W)} + \left(\frac{\partial \ln \gamma}{\partial W}\right)_{T_K,\ 1\ \text{atm}}\right\}\left\{(1-W)\left(\frac{\partial V}{\partial W}\right)^2_{T_K,\ 1\ \text{atm}}\right\}^{-1} \tag{113}$$

where R is the gas law constant, T_K is the absolute temperature in kelvin, V is the specific volume of the gradient-forming solute, γ is the molar activity coefficient and M is the molecular weight of the gradient-forming solute.

For 1:1 electrolytes, $\ln \gamma$ is a smooth function of $\sqrt{W}$, so

$$\frac{\partial \ln \gamma}{\partial W} = \frac{1}{2\sqrt{W}} \frac{\partial \ln \gamma}{\partial(\sqrt{W})}. \tag{114}$$

Numerical differentiation was carried out in most cases by fitting a 3rd degree polynomial by the method of least squares to 5 consecutive points of $(\ln \gamma, \sqrt{W})$.

For K_2tartrate and K_3citrate, the available activity data do not extend to a sufficiently low concentration to show the expected asymptotic behavior as $W \to 0$, and no attempt was made to impose such a behavior on the data.

Table 1 shows the source and range of the data, and the standard deviation of the data from the correlation. A discussion of some special cases follows.

Activity coefficients for CsCl solutions have been reported by Harned and Schupp [35], Robinson and Stokes [36], Caramazza [37], and Robinson [38]. Harned and Schupp, and Caramazza, used reversible cell emf measurements and their results agree closely with one another. Robinson and Stokes, and Robinson, used isopiestic measurements and their results also agree closely with one another. Unfortunately there is a divergence of the electrometric results from the isopiestic results at high concentrations. The cause of the discrepancy is not known, nor is it clear which results are most accurate. (Direct measurements of β^0 in a centrifuge by Ifft et al. [39] agree best with the isopiestic activities. It is not known, however, whether the centrifuge measurements are sufficiently accurate to be considered decisive in this case.) In the present work, the activity data of Caramazza have been used to calculate β^0, primarily because of the wide range of temperatures included. The values of β^0 obtained in this way deviate by as much as 15% from the values based on isopiestic activities reported by earlier investigators [10,29].

Diffusion coefficients for CsCl solutions were available only at 25°C. These values were adjusted for other temperatures using the equation of Gordon [40].

Activity coefficients for sucrose solutions were available only at 25°C. Heat of dilution data were available down to 12°C, and were used to adjust the activity coefficients to other temperatures. The heat of dilution data appeared to scatter appreciably, however, so the correction was considered suspect. An attempt was therefore made to calculate the osmotic pressure at 30°C and 0°C. The values thus obtained agreed with those reported by Berkeley et al. [41] within about 0.3%, up to a sucrose molality of 3.

Diffusion coefficients for sucrose were found over the range of 1 to 70°C and 0–70 wt%, but below room temperature, the only data were for very dilute solutions. All data were fit by least squares to a single equation using a parabolic dependence on mass fraction, and a dependence on temperature in the form of Antoine's equation [42]. The net effect of this procedure is that diffusion coefficients at low temperatures, and intermediate to high concentrations, are obtained by extrapolation of the higher temperature data using Antoine's equation [42].

The activity data reported by McDonald and Hsu [43] and used in the present work were not obtained by direct measurement, but rather were calculated from measured diffusion coefficients using an equation similar to Gordon's equation.

The experimental K_2tartrate density values of Martignoni [44] covered only a narrow range of concentration from 38 to 46% tartrate. Densities between 0 and 38% were obtained by interpolation. Because of the very wide gap between 0 and 38%, the data were first converted into ρ vs c (gms K_2tartrate/cc solution). A plot of these variables usually results in a more nearly straight line than other methods of correlation. A least-squares polynomial was fit to the ρ vs c data, and the results were then converted back to the form $W(\rho)$ needed in the present work.

In the case of K_3citrate and K_2tartrate, data for most properties were available only at 5 concentrations. In these cases an equation was fit exactly to all 5 points, so that no standard deviation estimate was obtained.

The thermodynamic parameter β^0 has been calculated and tabulated by a number of investigators. Comparison of the values obtained with the present work is discussed below.

For CsCl the comparison has already been mentioned.

Table 1
Gradient-forming solute properties

Property	Source	Range of data		Std. deviation
CsCl				
density	ICT [45]	$0°C \leq T \leq 30°C$	$0 \leq W \leq 0.65$	± 0.00006 wt. fraction units
viscosity	Lyons and Riley [46], Gmellins Handbook [47]	$0°C \leq T \leq 50°C$	$0 \leq W \leq 0.63$	± 2%
$(\partial \ln \gamma/\partial\sqrt{W})_{T,p}$	Caramazza [37]	$0°C \leq T \leq 35°C$	$0 \leq W \leq 0.5$	± 0.15 out of ~ 2.6 maximum
diffusivity	Robinson and Stokes [48]	$T = 25°C$ (see text for temperature correction)	$0 \leq W \leq 0.57$	± 0.4%
Sucrose				
density	Barber [49]	$0°C \leq T \leq 30°C$	$0 \leq W \leq 0.60$	± 0.04% density
viscosity	Barber [49]	$0°C \leq T \leq 30°C$	$0 \leq W \leq 0.60$	± 0.3%
activity	Robinson and Stokes [48], Hunter [50]	$12°C \leq T \leq 30°C$ (verified down to 0°C)	$0 \leq W \leq 0.60$	0.6% maximum deviation at 25°C. Unknown at other temperatures
diffusivity	English and Dole [51], Gosting and Morris [52], Henrion [53], Gladden and Dole [54]	$1°C \leq T \leq 70°C$ (but no data below room temperature when $W > 0.05$)	$0 \leq W \leq 0.70$	± 2%
KBr				
density	ICT [45]	$T = 25°C$	$0 \leq W \leq 0.40$	± 0.00005 mass fraction units
viscosity	Landolt–Bornstein [55]	$T = 25°C$	$0 \leq W \leq 0.40$	± 0.2%
$(\partial \ln \gamma/\partial\sqrt{W})_{T,p}$	Robinson and Stokes [48]	$T = 25°C$	$0 \leq W \leq 0.40$	± 0.02 units out of a maximum of 3
diffusivity	Robinson and Stokes [48]	$T = 25°C$	$0 \leq W \leq 0.36$	± 0.3%
NaBr				
density	Adams and Schumaker [56]	$T = 25°C$	$0 \leq W \leq 0.48$	0.00004 mass fraction units
viscosity	Adams and Schumaker [56]	$T = 25°C$	$0 \leq W \leq 0.48$	the original data are reported to be reproducible within ± 0.2%
activity	Robinson and Stokes [48], Penciner and Marcus [57]	$T = 25°C$	$0 \leq W \leq 0.50$	± 0.005 out of a maximum of 0.6 before differentiation
diffusivity	Robinson and Stokes [48]	$T = 25°C$	$0 \leq W \leq 0.22$	± 0.6%
K_3citrate				
density	Barber [58]	$T = 25°C$	$0 \leq W \leq 0.56$	indeterminate
viscosity	McDonald and Hsu [43]	$T = 25°C$	$0 \leq W \leq 0.50$	indeterminate
activity	McDonald and Hsu [43]	$T = 25°C$	$0 \leq W \leq 0.50$	indeterminate
diffusivity	McDonald and Hsu [43]	$T = 25°C$	$0 \leq W \leq 0.50$	indeterminate

Table 1 *continued*

Property	Source	Range of data		Std. deviation
K_2tartrate				
density	Martignoni [44]	$T = 25°C$	$0.38 \leq W \leq 0.46$	± 0.00015 mass fraction units
viscosity	McDonald and Hsu [43]	$T = 25°C$	$0 \leq W \leq 0.50$	indeterminate
activity	McDonald and Hsu [43]	$T = 25°C$	$0 \leq W \leq 0.50$	indeterminate
diffusivity	McDonald and Hsu [43]	$T = 25°C$	$0 \leq W \leq 0.50$	indeterminate

For sucrose at 25°C, β^0 has been calculated by Ifft, Voet, and Vinograd [11], Trautman [10], and McEwen [12], and a graph comparing the results has been presented by McEwen. All results appear to be consistent, and the values obtained in the present work, fall generally within the scatter band of previous results.

For KBr at 25°C, β^0 has been calculated by Ifft, Voet, and Vinograd [11], and by Ifft, Martin, and Kinzie [39]. The results agree well at lower concentration but deviate somewhat as the concentration is increased. Results of the present work agree much better with those of Ifft, Voet, and Vinograd despite the fact that the numerical analysis used (numerical differentiation by least squares polynomials) is more nearly similar to that of Ifft, Martin, and Kinzie.

For NaBr at 25°C, values of β^0 agree well with those of Ifft, Martin, and Kinzie [39] except at the highest concentration where a difference of about 8% occurs.

3. Comparison of simulated and physical results

This simulation methodology in the form of the computer program DIFSED has been used to evaluate and design separation protocols for zonal centrifugation. Selected examples from these studies which compare experimental and calculated results are used to assess the utility of this simulation method.

3.1. Lipoprotein flotation on a diffusion gradient

Separation of plasma lipoproteins in zonal rotors was first reported by Heimberg [59] and by Wilcox and Heimberg [60]. At that time, we set out to optimize these separations and consequently initiated development of this simulation method [61].

3.1.1. Materials and methods

Cesium chloride (99%) was obtained from Kawecki Berylco Industries, Inc., and purified before use by the method of Wright, Pappas, Carter, and Weber [62]. Sodium and potassium bromide were analytical reagent grade (Baker Chemical Co.). Human plasma was recovered from one unit of freshly drawn blood collected in ACD anticoagulant (kindly supplied by J.N. Brantley), and held at 4° under sterile conditions. All separations and analyses were performed with this sample to provide internal consistency in comparing simulated and experimental results. The "lipoprotein fraction" sample for zonal centrifugation containing those proteins with solvated density less than 1.20 g/cm^3, was prepared by diluting an aliquot of the above plasma [with 55% w/w CsCl, 0.01 M tris-HCl (pH 7.6), 0.005 M EDTA] to a density of 1.20 g/cm^3 neglecting protein. This solution was centrifuged in polycarbonate tubes at 50000 rpm and 20° in a Beckman Ti-50 angle-head rotor for 18 hrs. The top 2 ml from each tube were removed by gentle suction and pooled. For analytical ultracentrifugation, the various lipoprotein fractions were isolated from the whole plasma by sequential centrifugation [63].

Zonal centrifugation was in a titanium B-XV rotor [64] in a Beckman L-ZU centrifuge at 25 ± 2°. The rotor contents were eluted through a spectrophotometer flow cell monitored at 280 nm and collected in 40-ml fractions. The density of these fractions was determined either with a specific gravity digital recorder [65] for KBr, or with a refractometer (Bausch and Lomb, Abbe-3L) for CsCl. The equation of Ifft, Martin,

and Kinzie [39] related density to refractive index of CsCl solutions.

Sample band width expansion due to rotor loading/unloading and to anomalous zone broadening or droplet formation [66–70] was estimated by the following experiment: Into the rotor spinning at 1700 rpm, were introduced in order through the edge line: 1600 ml 0.05 M tris-HCl (pH 7.0); 33 ml sample [40 mg/ml bovine serum albumin (BSA), 0.05 M tris-HCl (pH 7.0); CsCl to a density of 1.20 g/cm^3]; 1850 ml cushion [0.05 M tris-HCl (pH 7.0), CsCl to a density of 1.50 g/cm^3]. The sample and 250 ml of the dense CsCl solution were metered into the rotor at 10 ml/min by a roller-tubing pump, then the remaining 1600 ml of dense solution was used to displace the rotor contents at 40 ml/min through a spectrophotometer flow cell in the rotor core line.

Analytical centrifugation was in a Beckman model E centrifuge using the schlieren optical system and the photoelectric scanner. Values of $\omega^2 t$ were obtained from a Beckman integrator attached to the photoelectronic speed control. Flotation occurred at 25 ± 0.5° in NaCl (1.063 g/cm^3) or NaBr (1.21 g/cm^3). Flotation coefficients were calculated from the minima of the schlieren curve or from the boundary half-height on the integral trace from the scanner, with the exception of the VLDL[‡] where three flotation coefficients were calculated (from the leading and trailing edges of the boundary, and from the half height) in an attempt to define the range of flotation coefficients among the VLDL. The scanner output was a 25 × 30 cm plot by a Hewlett–Packard X–Y recorder.

The physical parameters used to simulate the zonal flotation of various particles (table 2) were obtained from the following sources.

Lipoproteins: Flotation coefficients were measured on fractions obtained by sequential density fractionation [63]. The light absorbance at 280 nm of these fractions; corrected for dilution, was used to describe the concentration of each particle species in whole plasma or in the lipoprotein fraction. Diffusion coefficients were calculated from the experimentally determined flotation coefficients and the particle densities, assuming a spherical shape; then checked in the case of the LDL and HDL by a second calculation employing the particle density and molecular weight [56, 71].

Plasma proteins: The denser plasma proteins were represented by three particle classes: serum albumin, fibrinogen + γ-globulins, and orosomucoid + α_1-antitrypsin. The use of composite particle classes was

[‡] Abbreviations used: VLDL, very low density lipoprotein, $\rho < 1.019$ g/cm^3; LDL, low density lipoprotein, $\rho = 1.019$–1.063 g/cm^3; HDL, high density lipoprotein; HDL_2 ρ = 1.093 g/cm^3, HDL_3 $\rho = 1.148$ g/cm^3.

Table 2
Physical constants of simulated plasma components

Particle	Sedimentation coefficient (Svedbergs)	Density (g/cm^3)	Diffusion coefficient (Ficks)	Concentration ($A_{280\,nm}^{1\,cm}$)	
				ACD-plasma	Lipoprotein fraction $\rho < 1.2$ g/cm^3)
VLDL	– 160 [a]	0.95	0.8	0.3	1.1
	– 80 [a]	0.97	1.0	0.3	1.1
	– 20 [a]	0.99	1.6	0.3	1.1
LDL	– 6.60 [a]	1.036	2.2	1.32	5.00
HDL_2	– 3.94 [b]	1.093	4.1	0.59	2.22
HDL_3	– 2.72 [b]	1.149	5.4	0.96	3.61
Uric acid	0.25 [c]	1.41	60	2.88	1.99
Orosomucoid α_1-antitrypsin	3.35 [c]	1.534	5.21	2.62	–
Albumin	4.60 [c]	1.364	6.10	20.2	–
Fibrinogen γ-globulin	7.02 [c]	1.358	3.66	21.6	–

[a] $S_{f\,1.063}$, [b] $F_{1.21}$, [c] $S_{20,w}$.

an attempt to account for the majority of plasma protein mass while remaining within the limited number of particles species that could be treated by the computer program. The physical properties of these particles were obtained from literature compilations [72,73]. Concentration values used were average male levels, converted to absorbance at 280 nm by absorptivity values from the literature [72,74]. In the case of the fibrinogen + γ-globulins and the orosomucoid + α_1-antitrypsin composite particle classes, the values used to simulate the particle class were the means of the light absorbance-weighted physical parameters,

$$\bar{p}_c = \sum_i (A_i P_i) / \sum_i (A_i),$$

where A_i is the absorbance at 280 nm due to the ith particle species in the sample, and P_i is the physical parameter (i.e., ... $S_{20,w}$, $D_{20,w}$, etc.) of the ith species.

Uric acid: Chemical analysis yielded a plasma uric acid concentration of 4.4 mg/100 ml [75]. This is equivalent to an A^{1cm}_{280nm} of 2.9 using a molar absorptivity value of 11×10^3 liters mole^{-1} cm^{-1} for uric acid in aqueous solution at pH 7.0 (Dr. Carl A. Burtis, personal communication). This value was confirmed by centrifuging dilute ACD-plasma in the analytical ultracentrifuge for a time sufficient to completely sediment a 2 svedberg boundary, then scanning the cell at 280 nm.

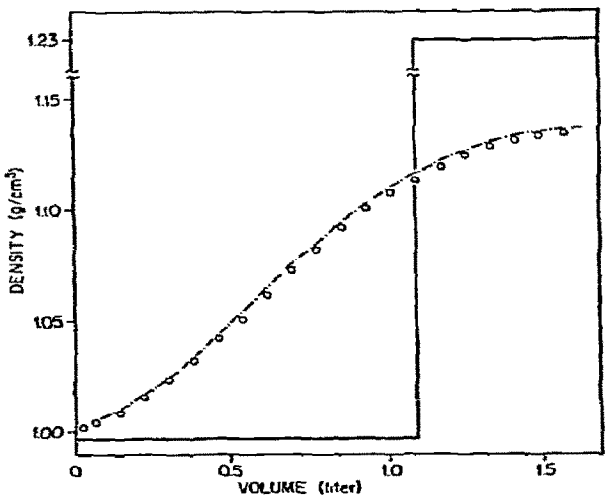

Fig. 1. KBr step gradient in B-XV rotor. Initial conditions (——), 25% radial gap step width. Calculated conditions (—·—·—·) and observed conditions (o o o) after 32.25 hours at 25° and 10000 rpm.

3.1.2. Results

The physical and simulated redistribution of a KBr step gradient at 10000 rpm are compared in fig. 1. Considering the non-ideality of the B-XV rotor cavity (non-radial septum surfaces and rounded corners at the outer wall), the experimental findings adequately confirm the calculated values. The same protocol with a narrower CsCl step gradient was used to determine if a relatively concentrated BSA sample zone would retard the diffusion of CsCl through the zone (fig. 2). No retardation was seen, thus confirming our earlier assumption that the macromolecules were sufficiently dilute to not af-

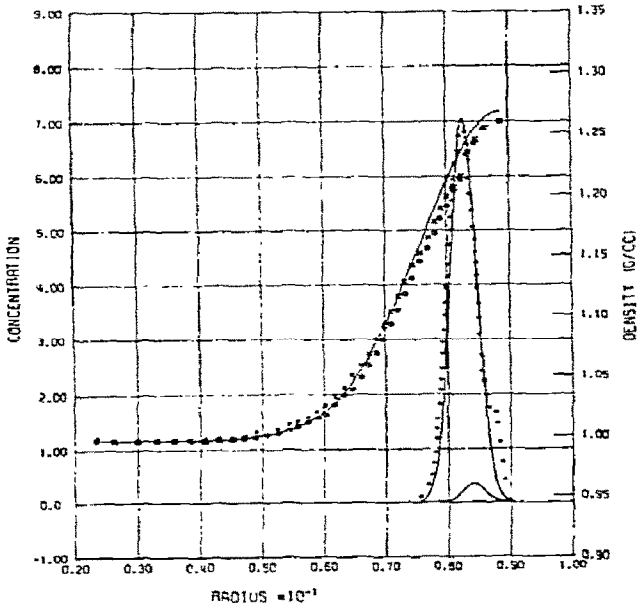

Fig. 2. CsCl step gradient in B-XV rotor with and without sample zone of bovine serum albumin. CsCl density gradient simulated (——), recovered from rotor without (o o o o o) and with (× × × × ×) BSA. BSA sample (including dimer) zone profile simulated (——) and experimental (● ● ● ● ●).

Initial gradient: with BSA, 1344 ml [0.01 M tris-HCl (pH 7.5)]; 33ml [sample containing 44 mg bovine serum albumin/ml, 0.01 M tris-HCl (pH 7.5), and 3 ml 0.01 M Tris-HCl (pH 7.5), CsCl to a density of 1.497 g/cm^3]; 290 ml [0.01 M tris-HCl (pH 7.5), CsCl to a density of 1.497 g/cm^3]. Without BSA, 1373 ml [0.01 M tris-HCl (pH 7.5)]; 293 ml [0.01 M tris-HCl (pH 7.5), CsCl to a density of 1.497 g/cm^3].

Simulated as: 2.4–7.97 cm rotor radius, 0.997 g/cm^3 gradient density; 7.97–8.01 cm, linear interpolation 0.997 to 1.043 g/cm^3; 8.01–8.06 cm, 1.043 g/cm^3; 8.06–8.10 cm, linear interpolation 1.043 to 1.497 g/cm^3, 8.10–8.89 cm, 1.497 g/cm^3 (sample zone 7.99–8.08 cm).

Rotor velocity: acceleration, 0.32 hr, 1500 to 25319 rpm; 9.11 hr at 25319 rpm; deceleration, 0.34 hr, 25319 to 1500 rpm.

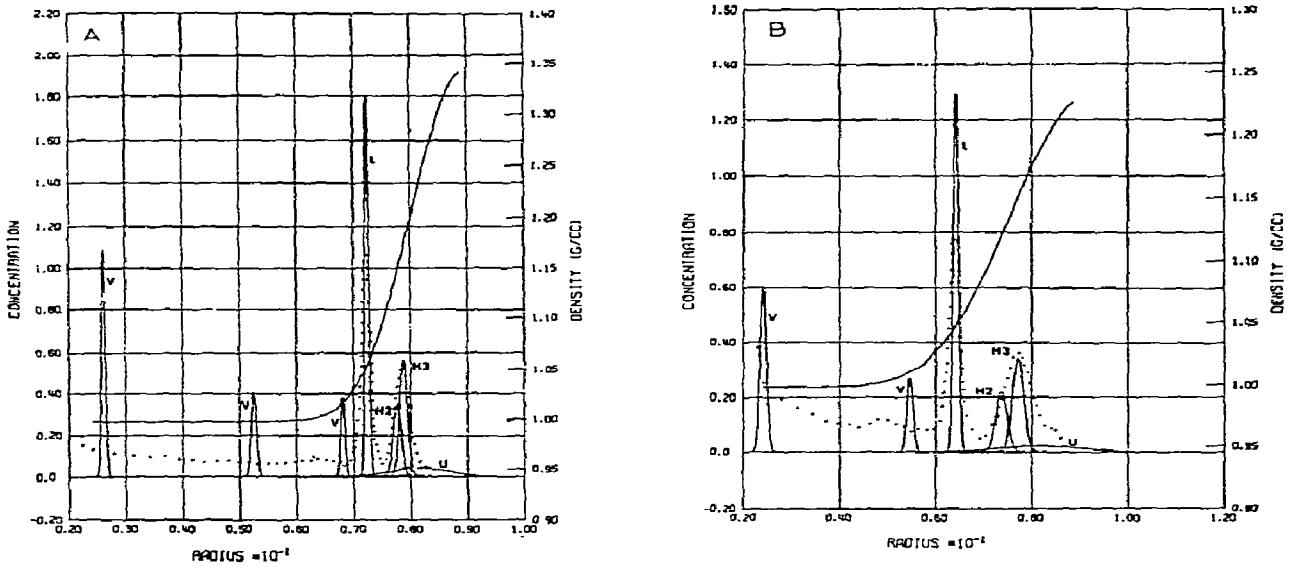

Fig. 3. Lipoprotein fraction centrifuged on a CsCl density step. Simulated (——), experimental (• • •).
Initial gradient: 1405 ml [0.05 M tris-HCl (pH 7.6), 0.005 M EDTA]; 11 ml [lipoprotein fraction]; 250 ml [0.05 M tris-HCl (pH 7.6), 0.005 M EDTA, CsCl to a density of 1.495 g/cm^3].
Simulated as: 2.4–8.12 cm rotor radius, 0.997 g/cm^3 gradient density; 8.12–8.23 cm, linear interpolation 0.997 to 1.495 g/cm^3; 8.23–8.89 cm, 1.495 g/cm^3. Sample zone: 8.13–8.18 cm radius.
Rotor velocity: (A) acceleration, 0.33 hr, 1500 to 27969 rpm; 3.84 hr at 27969 rpm; deceleration 0.33 hr, 27969 to 1500 rpm. (B) acceleration, 0.33 hr, 1500 to 25745 rpm; 14.03 hr at 25745 rpm; deceleration, 0.20 hr, 25745 to 1500 rpm.
Particle zone identification: V, VLDL; L, LDL; H2, HDL_2; H3, HDL_3; U, uric acid; A, albumin.

fect the behavior of the gradient-forming solute. The less rigorous match between the experimental CsCl redistributions and the simulated gradient than that found with KBr is due to the placement of the narrower initial salt gradient. The outer 10% of the rotor cavity's radius contains the rounded corners, which produce a smaller volume than that calculated from the simple cylindrical geometry used for simulation.

This degree of inaccuracy in gradient simulation does not appreciably affect the ability to predict macromolecule zone movement in the experimental gradient. Simulated and experimental separations of lipoproteins were compared using both the lipoprotein fraction and whole plasma samples. Lipoprotein fraction samples were centrifuged for 4.0 and 14.5 hr at 28 000 rpm on a CsCl step gradient (fig. 3a,b). Only the LDL and the combined HDL_2–HDL_3 zones could be clearly identified in the experimental gradient profile, and the center of each agreed closely with its predicted radial position. We did not expect to find peaks in the experimental trace corresponding to the three simulated VLDL peaks, since those three zones represented the two extremes and the midpoint of a very broad boundary in the analytical ultracentrifuge. A similar fractionation of plasma in the zonal rotor (fig. 4) showed the simulated and experimental LDL and HDL zone positions in agreement at 16.6 hr. The observed HDL zone was not as well resolved from the denser plasma proteins as predicted. Contributions to this apparent lack of agreement in fig. 4 include: (1) The small UV-absorbing plasma constituents (typified by uric acid in the simulated trace), which would tend to obscure separations. (2) We have not accounted for all particle species present in plasma, but have attempted to represent them within the limits of the simulation program. (3) There is actually more of the fibrinogen + γ-globulin peak present than shown in the Calcomp plots (e.g., to enable the computer to efficiently produce useable plots a small departure from reality is necessary. As the dense plasma proteins sediment onto the wall, or conversely, as the VLDL impact onto the rotor core, their concentration at the wall increases

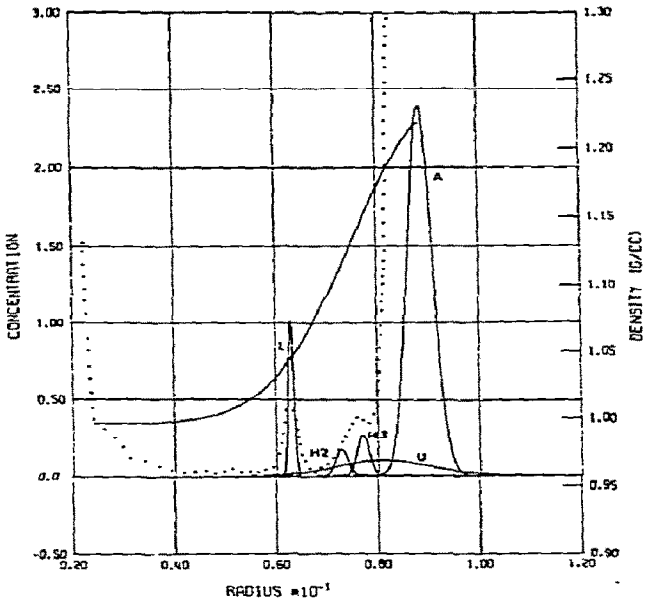

Fig. 4. ACD-plasma centrifuged on a CsCl density step. Simulated (——) experimental (• • •).

Initial gradient: 1383 ml [0.05 M tris-HCl (pH 7.6), 0.005 M EDTA]; 33 ml [sample containing 30 ml ACD plasma and 3 ml 0.05 M tris-HCl (pH 7.6), 0.005 M EDTA, CsCl to a density of 1.5 g/cm^3]; 250 ml [0.05 M tris-HCl (pH 7.6), 0.005 M EDTA, CsCl to a density of 1.5 g/cm^3].

Simulated as: 2.4–8.14 cm, 0.997 g/cm^3; 8.14–8.22 cm, linear interpolation 0.997 to 1.500 g/cm^3; 8.22 to 8.89 cm, 1.500 g/cm^3. Sample zone: 8.02–8.18 cm radius.

Rotor velocity: acceleration, 0.42 hr, 1500 rpm to 28094 rpm; 15.83 hr at 28094 rpm; deceleration, 0.33 hr, 28094 to 1500 rpm.

Particle zone identification as in fig. 3.

exponentially. To plot this concentration, the program would select a concentration range in which the zones of greater interest, i.e., HDL, uric acid, would be virtually invisible. This inconvenience is eliminated by allowing the particle zone to mathematically sediment through the wall until the zone center reaches the wall radius, at which time the plotting of that particular zone is suppressed. The zone concentration profile data is still tabulated in the printed output and can be added manually if desired. In the present case, the fibrinogen + γ-globulins zone center reached the rotor wall at 13 hr, and at the time plotted (16.6 hr, fig. 4) was calculated to contribute an absorbance of 0.5 $A^{1\text{ cm}}_{280\text{ nm}}$ at a radius of 8.80 cm). A further complication of a particle species actually compacting onto the rotor wall or core is that the back diffusion of that species will be enhanced by the increased particle concentration near the solid surface.

The observed LDL peaks were generally broader than predicted. This was not due to zone expansion caused by fluid mixing during the sample loading process, or transient density instabilities [66,69,70], as shown by inserting a BSA sample and CsCl gradient in the rotor; then immediately unloading it through a spectrophotometer flow cell (cf. Methods). The recovered protein peak appeared gaussian in shape with a width at half height almost twice that of the original sample. However, whether the inserted sample volume of 33 ml, or the immediately recovered sample volume of 60 ml was used to simulate initial conditions, the calculated lipoprotein peak widths resulting from one hour of centrifugation are identical within the limits of measurement. The major reason for the wider observed LDL zones in figs. 3 and 4 is probably the hydrodynamic heterogeneity of the lipoprotein particle populations.

These results (figs. 3 and 4) demonstrate that the radial location of particle zones sedimenting in a rapidly changing density gradient can be accurately predicted. The zone concentration profiles predicted from particle diffusion and from the effect on the zone of the solute density and viscosity gradients [76,77] agree reasonably well with experiment in figs. 3 and 4 considering the heterogeneity of the lipoproteins. This agreement is decreased near a rotor wall on which part of the particle zone has compacted.

3.2. Reorientation of CsCl gradients in the K-III rotor

Two characteristics of K-series centrifuge operation complicate the analysis of particle transport in these rotors. Loading and unloading of density gradients is generally performed with the rotor at rest [1]. This results in a gravitational reorientation of the gradient as the rotor is accelerated and decelerated, with isodense regions of the gradient passing through parabolae of revolution [78–80]. While the gradient reorientation into the cylindrical "spin" configuration is generally considered complete above 2000 rpm (because the greatest tendency for gradient mixing due to Coriolis force occurs below this velocity), in reality the gradient approaches asymptotically the cylindrical geometry assumed for simulation. This effect is appreciable only because of the length of

the K-rotors. Second, the narrow radial gap (1.2 cm) of the K-II and K-III rotors coupled with the large surface area between concentric volume elements of the gradient in "spin" configuration result in a rapid redistribution of gradient forming solute by diffusion. This has led to the general use of initial step gradients that rapidly diffuse during the separation. In the case of continuous-sample-flow operation this rapidly diffusing gradient solute may be lost from the rotor cavity into the exiting sample stream.

3.2.1. Methods

Cesium chloride was determined as for the lipoproteins. The titanium K-III rotor was used in a temperature controlled centrifuge as previously described [81, 82]. The initial density gradient was a CsCl step occupying the outer half of the radial gap. The rotor was filled at rest with deionized water at 25°C, then 1728 ml CsCl solution (1.3 g/cm^3) was pumped in through the lower fluid line (the volume of CsCl added was determined by weighing the water displaced from the rotor). The rotor was accelerated at 2 rpm/s to 500 rpm, and at 4 rpm/s to 2000 rpm, then at full drive air pressure to 35000 rpm. This operation required 25 minutes. After 1 hour at 3500 rpm, the rotor was decelerated under full braking air pressure to 2500 rpm, allowed to coast to 2000 rpm, then decelerated at 4 rpm/s to 500 rpm and at 2 rpm/s to rest. This operation also required 25 minutes. The gradient was immediately unloaded through the bottom line at 100 ml/min by air pressure.

3.2.2. Results

The close correspondence between the observed and simulated CsCl distributions (fig. 5) suggest that rapidly diffusing gradients of CsCl can be predicted with confidence even with reorientation in the K-III rotor when the acceleration–deceleration phases require 45% of the total time. We have not attempted to deal with the transient parabolic gradient configurations below 2000 rpm. A more complete study of diffusing gradients in the K-III rotor has earlier verified our ability to simulate the diffusion of gradient-forming solute into the continuous-flow stream at the rotor core and subsequent removal from the rotor [82].

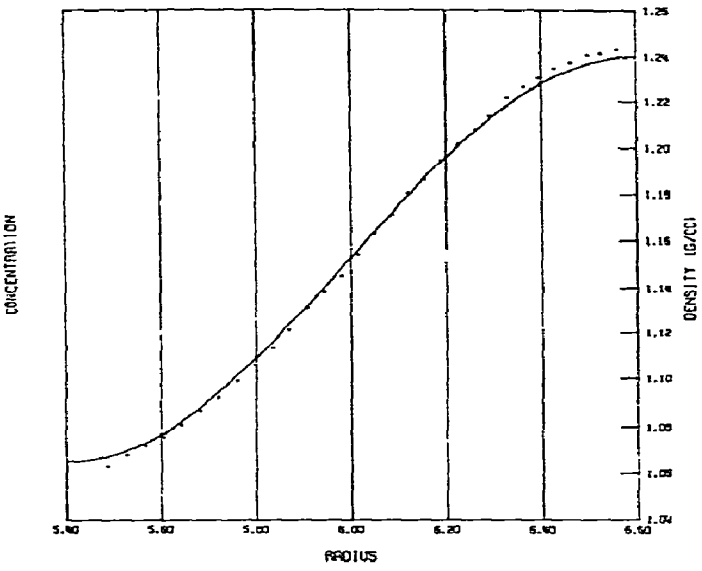

Fig. 5. CsCl gradient in K-III rotor. Experimental (• • •) and calculated (——) density gradient. Initial experimental conditions in text.

Simulated as: 5.4 to 5.997 cm rotor radius, 0.997 g/cm^3 gradient density; 5.997 to 6.003 cm, linear interpolation 0.997 to 1.3 g/cm^3; 6.003 to 6.6 cm, 1.3 g/cm^3.

Rotor velocity: 0.033 hr, linear interpolation 0 to 2000 rpm; 0.35 hr, linear interpolation 2000 to 35000 rpm; 1.0 hr, 35000 rpm; 0.384 hr, linear interpolation 35000 to 2000 rpm; 0.033 hr, linear interpolation 2000 to 0 rpm.

3.3. Concentration profiles of macromolecular zones

In the separation of macromolecular species by zonal centrifugation, the concentration profile (and especially the width) of the sedimenting bands, as well as the mean radius of the bands, must be known to determine the degree of separation. The stability of a band, which may determine the capacity, i.e., the maximum mass of macromolecules that can be loaded onto the gradient, also depends on the concentration profile during centrifugation [24,66–70,76–77].

While the present method includes the ability to simulate changes in macromolecule zone shape due to sedimentation through a supporting gradient of varying viscosity and density, and simultaneously to calculate band resolution and stability at each time step; here we specifically treat zone profiles resulting from macromolecular diffusion in a stable density gradient.

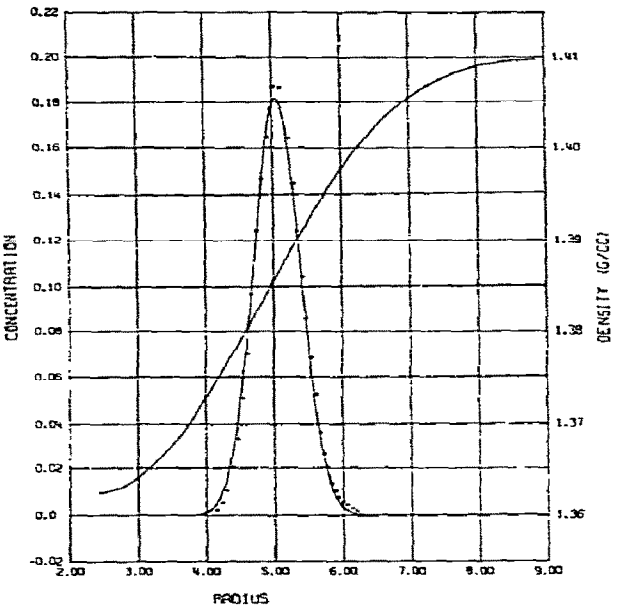

Fig. 6. Diffusion of cytochrome-c in NaBr. Simulated (——), experimental (• • •). Conditions as in [83].

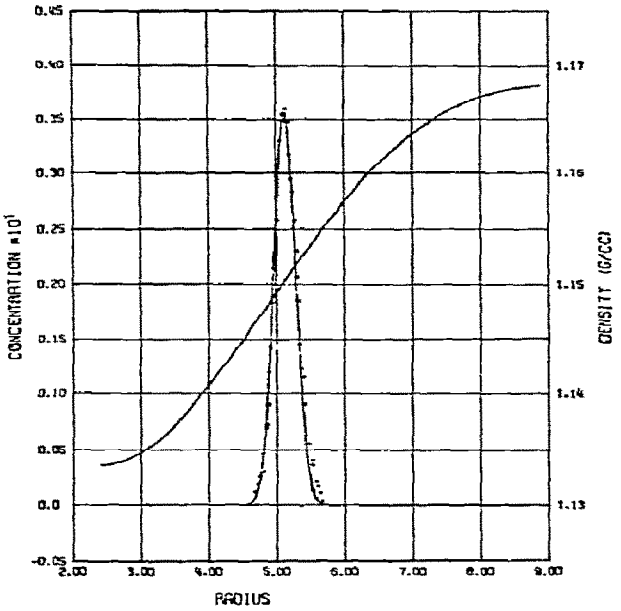

Fig. 8. Diffusion of MI3 viral DNA in NaBr. Simulated (——), experimental (• • •). Conditions as in [85].

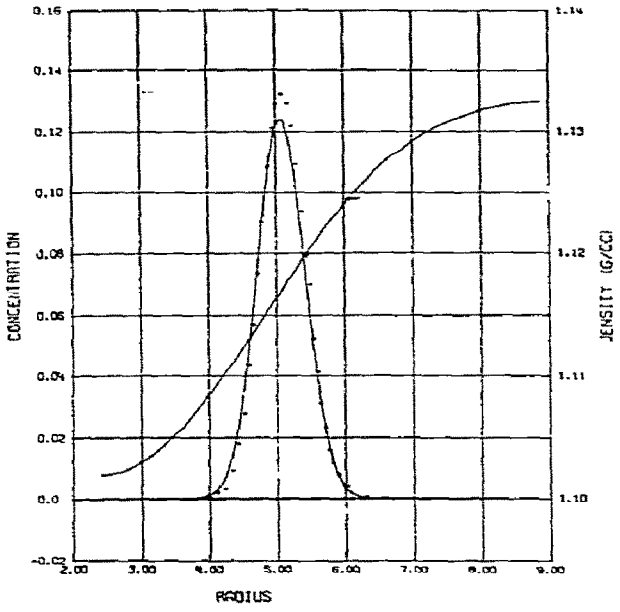

Fig. 7. Diffusion of bovine serum albumin in NaBr. Simulated (——), experimental (• • •). Conditions as in [84].

During the development of the technique of zonal diffusion, the diffusion coefficients of cytochrome-c, bovine serum albumin, and M13 viral DNA were determined from very careful measurements of the zone profiles resulting solely from diffusion (insofar as possible through experimental design) [83–85]. Selected cases from these studies have been simulated and compared in figs. 6–8. The fits obtained indicate that over a tenfold range of diffusion coefficient the simulated results reflect reality. The most difficult problem in comparing experimental and simulated results of this nature is determining the actual concentration (light absorption) of macromolecules inserted into the rotor, analogous to the problems experienced during analytical ultracentrifugation studies.

3.4. Particle sedimentation in band-forming centerpieces

The development of band-forming centerpieces for the analytical ultracentrifuge opened a valuable field of particle analysis [17]. The necessity that the sedimenting macromolecule band be supported on a shallow diffusion gradient has been met by appropriate choice of rotor speed. A more rigorous investigation

of band shape and position due to interaction with these dynamic gradients is within the scope of the present method. The band centrifugation studies with M13 viral DNA [85] have been simulated and compared with excellent correspondence.

References

[1] N.G. Anderson, D.A. Waters, C.E. Nunley, R.F. Gibson, R.M. Schilling, E.C. Denny, G.B. Cline, E.F. Babelay and T.E. Perardi, Anal. Biochem. 32 (1969) 460.
[2] M. Dishon, G.H. Weiss and D.A. Yphantis, Biopolymers 4 (1966) 449.
[3] M. Dishon, G.H. Weiss,and D.A. Yphantis, Biopolymers 4 (1966) 457.
[4] M. Dishon, G.H. Weiss and D.A. Yphantis, Biopolymers 5 (1967) 697.
[5] D.J. Cox, Arch. Biochem. Biophys. 112 (1965) 249.
[6] D.J. Cox, Arch. Biochem. Biophys. 112 (1965) 259.
[7] D.J. Cox, Arch. Biochem. Biophys. 119 (1967) 230.
[8] D.J. Cox, Arch. Biochem. Biophys. 129 (1969) 106.
[9] J.R. Cann and W.B. Goad, Science 170 (1970) 441.
[10] R. Trautman, Arch. Biochem. Biophys. 87 (1960) 289.
[11] J.B. Ifft, D.H. Voet and J. Vinograd, J. Phys. Chem. 65 (1961) 1138.
[12] C.R. McEwen, Anal. Biochem. 19 (1967) 23.
[13] R.G. Martin and B.N. Ames, J. Biol. Chem. 236 (1961) 1372.
[14] B.S. Bishop, in: The development of zonal centrifuges, National Cancer Institute Monograph 21, ed. N.G. Anderson (U.S. Govt. Printing Office, Washington, 1966) p. 175.
[15] M. Gehatia and E. Katchalski, J. Chem. Phys. 30 (1959) 1334.
[16] M.M. Rubin and A. Katchalski, Biopolymers 4 (1966) 579.
[17] J. Vinograd, R. Bruner, R. Kent and J. Weigle, Proc. Natl. Acad. Sci. U.S. 49 (1963) 902.
[18] M. Dishon, G.H. Weiss and D.A. Yphantis, Ann. N.Y. Acad. Sci. 164 (1969) 33.
[19] R.L. Baldwin and E.M. Shooter, in: Ultracentrifugal analysis, ed. J.W. Williams (Academic, New York, 1963) p. 143.
[20] J. Vinograd and R. Bruner, Biopolymers 4 (1966) 131.
[21] V.N. Schumaker and J. Rosenbloom, Biochem. 4 (1965) 1005.
[22] E. Kucera, J. Chromatography 19 (1965) 237.
[23] C. de Duve, J. Berthet and H. Beaufay, in: Progress in biophysics and biophysical chemistry 9, ed. J.A.V. Butler and B. Katz (Pergamon, London, 1959) p. 325.
[24] A.S. Berman, in: The development of zonal centrifuges, National Cancer Institute Monograph 21, ed. N.G. Anderson (U.S. Govt. Printing Office, Washington, 1966) p. 41.
[25] M. Dishon, G.H. Weiss and D.A. Yphantis, Biopolymers 10 (1971) 1095.
[26] G.H. Weiss and M. Dishon, Biopolymers 9 (1970) 865.
[27] T. Svedberg and K.O. Pederson, The ultracentrifuge (Oxford, London, 1940).
[28] G.J. Hooyman, H. Hilton, Jr., P. Mazur and S.R. DeGroot, Physica XIX (1953) 1095.
[29] J.E. Hearst, J.B. Ifft and J. Vinograd, Proc. Natl. Acad. Sci. U.S. 47 (1961) 1015.
[30] J. Crank and P. Nicholson, Proc. Cambridge Phil. Soc. 43 (1947) 50.
[31] O. Lamm, Ark. Mat. Astr. o. Fys. 21B (1929) Nr. 2.
[32] E.F. Eikenberry, T.A. Bickle, R.R. Traut and C.A. Price, Eur. J. Biochem. 12 (1970) 113.
[33] M. Abramowitz and I.A. Stegum, Handbook of mathematical functions with formulas, graphs, and mathematical tables (U.S. Govt. Printing Office, Washington, 1964).
[34] V.N. Schumaker, Separation Sci. 1 (1966) 409.
[35] H.S. Harned and O.E. Schupp, Jr., J. Am. Chem. Soc. 52 (1930) 3886.
[36] R.A. Robinson and R.H. Stokes, Trans. Faraday Soc. 45 (1949) 612.
[37] R. Caramazza, Ann. Chim. (Rome) 53 (1963) 481.
[38] R.A. Robinson, J. Am. Chem. Soc. 74 (1952) 6035.
[39] J.B. Ifft, W.R. Martin, III and K. Kinzie, Biopolymers 9 (1970) 597.
[40] A.R. Gordon, J. Chem. Phys. 5 (1937) 522.
[41] Lord Berkeley, E.G. J. Hartley and C.V. Burton, Phil. Trans. 218A (1919) 295.
[42] Ch. Antoine, Compt. rend. 107 (1888) 681, 836.
[43] D.M. McDonald and H.W. Hsu, Separation Sci. 7 (1972) 491.
[44] M.E. Martignoni, personal communication, June 16, 1972.
[45] E.W. Washburn, International critical tables (McGraw–Hill, New York, 1926).
[46] P.A. Lyons and J.F. Riley, J. Am. Chem. Soc. 76 (1954) 5216.
[47] Gmelins handbuch der anorganishe chemie (Verlag Chemie Leipzig–Berlin, 1926).
[48] R.A. Robinson and R.H. Stokes, Electrolyte solutions (Butterworths, London, 1955).
[49] E.J. Barber, in: The development of zonal centrifuges, National Cancer Institute Monograph 21, ed. N.G. Anderso (U.S. Govt. Printing Office, Washington, 1966) p. 219.
[50] R.M. Hunter, Trans. Faraday Soc. 22 (1926) 194.
[51] A.C. English and M. Dole, J. Am. Chem. Soc. 7 (1950) 3261.
[52] L.J. Gosting and M.S. Morris, J. Am. Chem. Soc. 71 (1949) 1998.
[53] P.N. Henrion, Trans. Faraday Soc. 60 (1964) 72.
[54] J.K. Gladden and M. Dole, J. Am. Chem. Soc. 75 (1953) 3900.
[55] Landolt-Bornstein, II Band, 5 Teil (Springer, Berlin, 1969).
[56] G.H. Adams and V.N. Schumaker, Anal. Biochem. 29 (1969) 117.
[57] J. Penciner and Y. Marcus, J. Chem. Eng. Data 10 (1965) 105.
[58] E.J. Barber, personal communication.

[59] M. Heimberg, Oak Ridge National Laboratory Report 4171 Special (1967) p. 72.
[60] H.G. Wilcox and M. Heimberg, Biochim. Biophys. Acta 152 (1968) 424.
[61] J. Breillatt and W.K. Sartory, Hydrodynamics of Plasma Lipoprotein Isolation in Zonal Rotors, presented at Lipoprotein Workshop, Biophysical Society 13th Annual Meeting, Los Angeles, California, February 28, 1969.
[62] R.R. Wright, W.S. Pappas, J.A. Carter and C.W. Weber, National Cancer Institute Monograph 21 (1966) 241.
[63] B. Shore, Arch. Biochem. Biophys. 71 (1957) 1.
[64] N.G. Anderson, D.A. Waters, W.D. Fisher, G.B. Cline, C.E. Nunley, L.H. Elrod and C.T. Rankin, Jr., Anal. Biochem. 21 (1967) 235.
[65] H.A. Kermicle and J. Farquharson, Oak Ridge Gaseous Diffusion Plant Report K-L-6171 (1967).
[66] S.P. Spragg, Resolution in Zonal Rotors, in: Particle Separation from Plant Materials, USAEC Report CONF-700119 (1970) pp. 81–88.
[67] H. Svensson, L. Hagdahl and K.D. Lerner, Sci. Tools 4 (1957) 1.
[68] S.P. Spragg and C.T. Rankin, Jr., Biochim. Biophys. Acta 141 (1967) 164.
[69] P. Nason, V.N. Schumaker, H.B. Halsall and J. Schwedes, Biopolymers 7 (1969) 241.
[70] W.K. Sartory, Biopolymers 7 (1969) 251.
[71] A.V. Nichols, Adv. Biol. Med. Physics 11 (1967) 109.
[72] H.E. Schultze and J.F. Heremans, Molecular Biology of Human Proteins Vol. I (Elsevier, Amsterdam 1966) p. 176–235.
[73] M.H. Smith, in: Handbook of Biochemistry, 2nd Ed., ed. H.A. Sober (Chemical Rubber Co., Cleveland, 1970) p. C–3.
[74] D.M. Kirschenbaum, in: Handbook of Biochemistry, 2nd Ed., ed. H.A. Sober (Chemical Rubber Co., Cleveland, 1970) p. C-71.
[75] R.A. Brown and E. Freier, Clin. Biochem. 1 (1967) 154.
[76] V.N. Schumaker, Separation Sci. 1 (1966) 409.
[77] S.P. Spragg, R.S. Morrod and C.T. Rankin, Jr., Separation Sci. 4 (1969) 467.
[78] T.E. Perardi, R.A.A. Leffler and N.G. Anderson, Anal. Biochem. 32 (1969) 495.
[79] N.G. Anderson, C.A. Price, W.D. Fisher, R.E. Canning and C.L. Burger, Anal. Biochem. 7 (1964) 1.
[80] H.W. Hsu and N.G. Anderson, Biophys. J. 9 (1969) 173.
[81] J.N. Brantley, D.D. Willis, J.P. Breillatt, R.F. Gibson, L.C. Patrick and N.G. Anderson, Anal. Biochem. 36 (1970) 434.
[82] J. Breillatt, W.K. Sartory and J.N. Brantley, Separation Method Design by Simulation Techniques: CsCl Gradients in the K-III Rotor, USAEC Report ORNL-TM-3185 (1971).
[83] H.B. Halsall and V.N. Schumaker, Biochem. Biophys. Res. Comm. 39 (1970) 479.
[84] H.B. Halsall and V.N. Schumaker, Biochem. Biophys. Res. Comm. 43 (1971) 601.
[85] H.B. Halsall and V.N. Schumaker, Biochemistry 11 (1972) 4692.